

1 **Centroid moment tensor inversions of offshore earthquakes using a three-**
2 **dimensional velocity structure model: Slip distributions on the plate**
3 **boundary along the Nankai Trough**

4
5 **Authors**

6 **Shunsuke TAKEMURA^{1*}, Ryo OKUWAKI², Tatsuya KUBOTA³, Katsuhiko SHIOMI³**
7 **Takeshi KIMURA³, Akemi NODA⁴**

8 ¹**Earthquake Research Institute, the University of Tokyo, 1-1-1 Yayoi, Bunkyo-ku,**
9 **Tokyo, 113-0032, Japan**

10 ²**Faculty of Life and Environmental Sciences, University of Tsukuba, 1-1-1 Tennodai,**
11 **Tsukuba 305-8572, Japan.**

12 ³**Network Center for Earthquake, Tsunami and Volcano, National Research Institute**
13 **for Earth Science and Disaster Resilience, 3-1 Tennodai, Tsukuba, Ibaraki, 305-0006,**
14 **Japan.**

15 ⁴**Earthquake and Tsunami Research Division, National Research Institute for Earth**
16 **Science and Disaster Resilience, 3-1 Tennodai, Tsukuba, Ibaraki, 305-0006, Japan.**

17
18
19
20 **Running Title**

21 3D CMT inversion along the Nankai Trough

22
23 **Corresponding Author**

24 Shunsuke Takemura

25 E-mail: shunsuke@eri.u-tokyo.ac.jp

26 Phone: +81 3-5841-5689

27

28 **Summary**

29 Due to complex three-dimensional (3D) heterogeneous structures, conventional one-
30 dimensional (1D) analysis techniques using onshore seismograms can yield incorrect
31 estimation of earthquake source parameters, especially dip angles and centroid depths of
32 offshore earthquakes. Combining long-term onshore seismic observations and numerical
33 simulations of seismic wave propagation in a 3D model, we conducted centroid moment
34 tensor (CMT) inversions of earthquakes along the Nankai Trough between April 2004 and
35 August 2019 to evaluate decade-scale seismicity. Green's functions for CMT inversions of
36 earthquakes with moment magnitudes of 4.3–6.5 were evaluated using finite-difference
37 method simulations of seismic wave propagation in the regional 3D velocity structure model.
38 Our CMT solutions were generally better than those in the catalogue based on regional 1D
39 analysis, especially for offshore earthquakes. By introducing the 3D structures of the low-
40 velocity accretionary prism and the Philippine Sea Plate, dip angles and centroid depths for
41 offshore earthquakes were well-constrained. Our 3D CMT catalogue and published slow
42 earthquake catalogues depicted spatial distributions of slip behaviours on the plate boundary
43 along the Nankai Trough. The regular and slow interplate earthquakes were separately
44 distributed, with these distributions reflecting the heterogeneous distribution of effective
45 strengths along the Nankai Trough plate boundary. By comparing the spatial distribution of
46 seismic slip on the plate boundary with the slip-deficit rate distribution, regions with strong
47 coupling were clearly identified.

48

49 **Keywords:**

50 Nankai Trough, seismicity, centroid moment tensor inversion, heterogeneous structure, finite-
51 difference method

52

53 1. Introduction

54 The earthquake focal mechanism is one of the most important parameters characterising
55 earthquake faulting. Focal mechanisms and their spatial distributions are important for
56 evaluating tectonic/local stress and strain fields (e.g. Townend & Zoback 2006, Terakawa &
57 Matsu'ura 2010, Saito *et al.* 2018). To determine focal mechanisms, first-*P* or *S* polarisation
58 inversion (e.g. Hardebeck & Shearer 2002, Thurber *et al.* 2006, Shelly *et al.* 2016) and
59 waveform-based centroid moment tensor (CMT) inversion (e.g. Dziewonski *et al.* 1981,
60 Kanamori & Rivera 2008, Vallée *et al.* 2011, Ekström *et al.* 2012) techniques have been
61 widely used in the world. One-dimensional (1D) Earth models are assumed in typical focal
62 mechanism determination methods. In regions with complex three-dimensional (3D)
63 heterogeneous structures, first-motion solutions using the 1D Earth model systematically
64 show mis estimations (e.g. Takemura *et al.* 2016). Although CMT methods based on long-
65 period (> 10 s) waveforms can be applicable only for moderate-to-large earthquakes due to
66 signal-to-noise problems for long-period components, their evaluations of source parameters
67 are generally robust against structural heterogeneities in comparison to first-motion solutions.

68 Along the Nankai Trough, megathrust earthquakes have repeatedly occurred at intervals of
69 100–150 years (e.g. Ando 1975). Evaluating seismicity around this region is important for
70 contributing to the understanding of megathrust earthquakes, such as evaluating stress
71 accumulation/release processes on plate boundaries. In Japan, regular and slow earthquakes
72 have been systematically monitored by the seismic networks of the Monitoring of Waves on
73 Land and Seafloor (MOWLAS; <https://doi.org/10.17598/NIED.0009>) operated by the
74 National Research Institute for Earth Science and Disaster Resilience (NIED; Okada *et al.*
75 2004). According to the combined earthquake catalogues of the International Seismological
76 Centre-Global Earthquake Model (ISC-GEM; Storchak *et al.* 2013), the Japan Meteorological
77 Agency (JMA), and the NIED F-net (Fukuyama *et al.* 1998, Kubo *et al.* 2002), the seismicity
78 of regular earthquakes along the Nankai Trough, especially interplate earthquakes, is quite
79 low. Figure 1 shows the spatial distribution of regular earthquakes with moment magnitudes
80 (M_w) of 4.3–6.5 that occurred from April 2004 to August 2019, as listed in the F-net moment
81 tensor (F-net MT) catalogue. A few shallow offshore earthquakes occurred in the Tonankai
82 and Nankai regions and their focal mechanisms in the F-net catalogue were not characterised
83 by low-angle thrust faulting. In other words, no earthquakes suggesting faulting on the plate
84 boundary around the Tonankai and Nankai regions are listed in the F-net MT catalogue.

85 On 1 April 2016, the M_w 5.8 earthquake, called “2016 southeast off the Kii Peninsula

86 earthquake”, occurred in the Tonankai region (marked A in Figure 1). The F-net MT solution
87 of this earthquake was characterised by high-angle (38°) reverse faulting below the upper
88 surface of the Philippine Sea Plate, indicating it was an intraslab earthquake. However, a
89 detailed analysis of this earthquake revealed that it could be modelled by a low-angle thrust
90 faulting at a depth of approximately 10 km, suggesting seismic slip along the plate boundary
91 (e.g. Wallace *et al.* 2016, Nakano, Hyodo, *et al.* 2018, Takemura, Kimura, *et al.* 2018).
92 Source models suggested in these studies were also consistent with a model based on
93 observed tsunami data (Kubota *et al.* 2018). In regions with a thick accretionary prism,
94 characteristics of surface wave propagation are significantly affected by a low-velocity
95 accretionary prism (e.g. Shapiro *et al.* 1998, Furumura *et al.* 2008, Nakamura *et al.* 2015,
96 Volk *et al.* 2017, Gombert 2018, Kaneko *et al.* 2019). Thus, the focal mechanisms of other
97 offshore earthquakes along the Nankai Trough could be incorrectly estimated using
98 conventional 1D regional MT inversion, even for long-period displacements. Indeed, shallow
99 very low frequency earthquakes along the Nankai Trough have been interpreted as low-angle
100 thrust faulting on the plate boundary by using offshore seismic observations (e.g. Sugioka *et*
101 *al.* 2012, Nakano, Hori, *et al.* 2018), but their focal mechanisms based on 1D analysis of
102 onshore observations were high-angle reverse faulting mechanisms within the accretionary
103 prism (Ito & Obara 2006). To evaluate seismic activity along the Nankai Trough more
104 precisely, offshore earthquakes listed in the previous 1D catalogues require re-analysis.

105 Parallel simulation codes of seismic wave propagation (e.g. Gokhberg & Fichtner 2016,
106 Maeda *et al.* 2017) and 3D seismic velocity structure models (e.g. Nishida *et al.* 2008,
107 Eberhart-Phillips *et al.* 2010, Koketsu *et al.* 2012) enable the simulation of Green’s functions
108 propagating through realistic 3D Earth models (hereafter called ‘3D Green’s functions’),
109 which have been used to develop CMT inversions (e.g. Ramos-Martínez & McMechan 2001,
110 Lee *et al.* 2013, Hejrani *et al.* 2017, Okamoto *et al.* 2018, Takemura, Kimura, *et al.* 2018,
111 Takemura, Matsuzawa, *et al.* 2018, 2019, Wang & Zhan 2019). Although the resolution of
112 detailed source characteristics for offshore earthquakes deriving using the 3D CMT method
113 and onshore seismograms are limited compared to those using offshore observations, these
114 methods provide similar focal mechanisms and centroid locations. Thus, offshore seismic
115 activity, including earthquakes before offshore seismic observations, can be effectively
116 evaluated.

117 To investigate the decade-scale seismicity of offshore earthquakes along the Nankai
118 Trough, we re-evaluated focal mechanisms based on CMT inversion using 3D Green’s

119 function datasets, which were evaluated by numerical simulations of seismic wave
120 propagation in a regional 3D velocity structure model. Then, to investigate spatial variation in
121 slip behaviours on the plate boundary along the Nankai Trough, we compared the spatial
122 distribution of focal mechanisms based on the 3D CMT technique with the spatial
123 distribution of slip-deficit rates (Noda *et al.* 2018), slow slip events (SSEs; Miyazaki *et al.*
124 2006, Nishimura *et al.* 2013, Kobayashi 2014, Takagi *et al.* 2016, 2019, Yokota & Ishikawa
125 2019), shallow low-frequency tremors (LFTs; Yamashita *et al.* 2015), shallow very low-
126 frequency earthquakes (VLFEs; Takemura, Noda, *et al.* 2019), and the 1968 Hyuga-nada
127 earthquake (Yagi *et al.* 1998).

128

129 **2. Data and Methods**

130 We used three-component velocity seismograms of F-net (National Research Institute for
131 Earth Science and Disaster Resilience 2019), the sensors of which have been systematically
132 monitored (Kimura *et al.* 2015). To conduct CMT inversion of the target earthquakes, we
133 applied a band-pass filter with passed periods of 25–100 s to velocity seismograms. We
134 selected a 25–100 s period band because ground motions for periods of 8–20 s are
135 significantly affected by internal structures of the accretionary prism along the Nankai
136 Trough (e.g. Nakamura *et al.* 2015, Guo *et al.* 2016, Takemura, Kimura, *et al.* 2018,
137 Takemura, Kubo, *et al.* 2019). We obtained displacement waveforms by calculating time
138 integration of each filtered velocity record. The target earthquakes occurred within the region
139 of assumed source grids (grey crosses in Figure 2) between April 2004 and August 2019, and
140 values of M_w in the F-net catalogue ranging from 4.3 to 6.5. According to the signal-to-noise
141 ratios for the target period band, the magnitude range of the analysed earthquake was
142 determined by trial and error. Source grids were uniformly distributed at horizontal intervals
143 of 0.1° . Depths of source grids ranged from 6 to 50 km at an interval of 2 km. The total
144 number of source grids was 61,433.

145 Green's functions were evaluated by solving equations of motion in the 3D viscoelastic
146 medium model based on the finite-difference method (FDM) simulations. The 3D simulation
147 model covered an area of $900 \times 1,000 \times 100 \text{ km}^3$, which was discretised by grid intervals of
148 0.5 km in the horizontal direction and 0.2 km in the vertical direction. We used a parallel
149 simulation code of OpenSWPC (Maeda *et al.* 2017), which includes the reciprocal calculation
150 mode for effectively evaluating Green's functions. The reciprocal calculation has proved very
151 useful in the case that the number of seismic source grids is significantly larger than the

152 number of seismic stations (e.g. Eisner & Clayton 2001, Petukhin *et al.* 2016, Hejrani *et al.*
153 2017, Okamoto *et al.* 2018). We obtained a total of approximately 35,000,000 Green's
154 function SAC files from 61,433 source grids to 32 F-net stations (black and blue filled
155 triangles in Figure 2) via 96 reciprocal FDM calculations. The source time function of each
156 Green's function was the Küpper wavelet with a duration of 1 s.

157 The 3D velocity model of Koketsu *et al.* (2012) was used, as it has been widely applied in
158 studies of seismic ground motions across Japan (e.g. Iwaki *et al.*, 2018; Miyazawa, 2019;
159 Park & Ishii, 2018; Takemura *et al.*, 2017). The topography model in our simulations was the
160 ETOPO1 model (Amante & Eakins 2009). The P - and S -wave velocities and density (V_P , V_S
161 and ρ) in the seawater layer were 1.5 km/s, 0.0 km/s and 1.04 g/cm³, respectively. The air
162 column was modelled as a vacuum with V_P of 0.0 km/s, V_S of 0.0 km/s and ρ of 0.001 g/cm³.
163 The minimum V_S in the solid column of 1.5 km/s was assumed. Simulations were conducted
164 using the computer system of the Earthquake and Volcano Information Center at the
165 Earthquake Research Institute, the University of Tokyo. Each simulation required 385
166 GBytes of computer memory and a wall-clock time of 2.5 hours and was performed using
167 parallel computing with 432 cores to evaluate seismic wave propagation of 200 s with 20,000
168 time-step calculations. According to our grid and model settings, our FDM simulation can
169 precisely evaluate long-period (> 10 s) seismic wave propagation.

170 Examples of Green's functions are illustrated in the right panels of Figure 2. The source
171 (red star) was located at a depth of 10 km, near the plate boundary. We employed the
172 Cartesian coordinate system of Aki & Richards (2002), where x , y , and z are taken as north,
173 east, and down, respectively. Due to the low-velocity accretionary prism and seawater,
174 durations of surface waves were amplified and elongated. In particular, where $M_{xy} = 1.0$ (i.e. a
175 pure strike-slip with strike angle of 0°, dip angle of 90°, and rake angle of 0°), Love waves in
176 horizontal components were strong and long. We assumed six-element moment tensors for
177 the CMT inversions, which includes five double couple and an isotropic moment tensors (e.g.
178 Kikuchi & Kanamori 1991).

179 In the CMT inversions, we basically used Green's functions at F-net stations within
180 epicentral distances of 100–400 km from the initial epicentre. The initial epicentre was
181 obtained from the F-net MT catalogue. In cases where earthquake $M_w < 4.5$, we selected a
182 distance range of 100–350 km due to the signal-to-noise ratio of the observed waveforms for
183 the analysed period. We visually checked the filtered displacement waveforms and discarded
184 noisy ones. Centroid location and time of the analysed earthquake were determined using grid

185 search inversion (e.g. Lee et al., 2014; Takemura, Matsuzawa, et al., 2019; Tsuruoka et al.,
186 2009). Because the analysis period range was longer than the source durations of target
187 earthquakes with $M_w = 4.3\text{--}6.5$, we did not estimate source durations of these events. A set of
188 Green's functions at the source grids, which were located in a $\pm 0.4^\circ$ region from the initial
189 epicentre and were distributed at depths of 6–50 km, was selected for the grid search
190 inversion.

191 The CMT inversions were conducted for each selected source grid every 1 s from three
192 minutes before the origin minute as recorded in the F-net catalogue. We used a 200-s time
193 window for each CMT inversion. After CMT inversion at all of the selected source grids, to
194 identify the optimal solution, we evaluated variance reductions (VRs) between the observed
195 and synthetic displacement seismograms for periods of 25—100 s. The VR could then be
196 evaluated using the following equation:

$$VR = \left[1 - \frac{\sum_{i=1}^{N_S} \int (u_i^{Obs.}(t) - u_i^{Syn.}(t))^2 dt}{\sum_{i=1}^{N_S} \int (u_i^{Obs.}(t))^2 dt} \right] \times 100 [\%] \quad (1)$$

197 where N_S is the number of stations and $u_i^{Obs.}$ and $u_i^{Syn.}$ are the time-series of observed and
198 synthetic displacements, respectively. If observed and synthetic seismograms are perfectly
199 matched, VR is 100 %. The solution with the maximum VR was considered the optimal
200 solution, providing the optimal centroid location, depth, time, focal mechanism, and seismic
201 moment of each earthquake. In the case that the optimal solution was located at the edges of
202 the initial assumed grid set, we performed the CMT inversion again using Green's functions
203 for a broader source grid dataset. Our grid search CMT inversion required approximately 15–
204 20 minutes using a typical, single-core desktop machine.

205

206 3. Results

207 We obtained a total of 215 CMT solutions for moderate earthquakes that occurred between
208 April 2004 and August 2019. We discarded the solutions with a maximum VR of less than
209 20%. Our 3D CMT catalogue was described in Global CMT (GCMT) format and listed in the
210 Supplementary data (Table S1). The size distribution and magnitude-time diagram of our 3D
211 CMT catalogue are shown in Figures S1 and S2. We note that the optimal solutions at the
212 edges of assumed all source grids may include some shifts outside the edges of the assumed
213 source grids (Figure 2). These earthquakes (at grid edges) were concentrated around southern
214 Kyushu and eastern edge of Izu.

215 Figures 3 and 4 show examples of CMT solutions for southeast off the Kii Peninsula

216 earthquake (1 April 2016) and the Hyuga-nada earthquake (10 May 2019), respectively. In
217 our previous study (Takemura, Kimura, *et al.* 2018), the 2016 southeast off the Kii Peninsula
218 earthquake was also analysed. The epicentre location and origin time were fixed in the
219 previous study. We re-analysed this earthquake via full 3D CMT inversion, which estimates
220 centroid location, depth, time, and moment tensor. The F-net MT solution of this earthquake
221 was a high-angle (38°) reverse faulting mechanism (grey focal sphere in Figure 3). Its
222 optimal solution is a M_w 5.9 low-angle (10.1°) thrust faulting at a depth of 10 km (Figure 3),
223 where the plate boundary closely exists (e.g. Kamei *et al.*, 2012; Park *et al.*, 2010). The
224 synthetic seismograms of the optimal solution corresponded well with the observations. The
225 depth variation of VRs illustrated a clear peak around the optimal depth. The centroid depth
226 of this earthquake was well constrained by our CMT inversion. Takemura, Kimura, *et al.*
227 (2018) numerically demonstrated that the low-velocity accretionary prism just above the
228 seismic source—which controls long-period surface wave propagation—provides a better
229 constraint on the centroid depth. According to the estimated focal mechanism and centroid
230 depth, this earthquake was considered as the faulting on the plate boundary. Furthermore, the
231 CMT result was consistent with models estimated by offshore observations (Wallace *et al.*
232 2016, Kubota *et al.* 2018, Nakano, Hyodo, *et al.* 2018).

233 Figure 4 shows the results of the CMT inversion and waveform fitting for the off the
234 Hyuga-nada earthquake on 10 May 2019. The F-net MT solution was also a high-angle (33°)
235 reverse faulting. The optimal CMT solution indicated a M_w 6.2 low-angle (15.6°) thrust
236 faulting. The dip angle agreed well with that of the Philippine Sea Plate around this
237 earthquake (e.g. Nakajima & Hasegawa 2007, Koketsu *et al.* 2012). The synthetic waveforms
238 also corresponded well to observed ones. Although the optimal depth (26 km) was
239 determined to be close to the upper surface of the Philippine Sea Plate (approximately 27
240 km), a high VR ($> 80\%$) area was found within a wider depth range (16–32 km). Because the
241 depth of this earthquake was deeper than the 2016 southeast off the Kii Peninsula earthquake,
242 the effects of the low-velocity accretionary prism might not have been so strong. Thus, the
243 depth resolution of the CMT solutions might not be good when compared to the case of the
244 2016 southeast off the Kii Peninsula earthquake. To constrain the hypocentre depth more
245 sharply, additional data, such as shorter-period (~ 4 s) first-arrival P -wave waveforms, would
246 need to be considered (e.g. Okamoto *et al.* 2018, Takemura, Kimura, *et al.* 2018, Wang &
247 Zhan 2019).

248 Figure 5 shows a comparison of the estimated focal mechanisms for the F-net and our 3D

249 CMT catalogues. Our CMT solutions of earthquakes in onshore regions were not
250 significantly different from the F-net ones. However, our CMT solutions differed to those
251 based on 1D analysis. In particular, dip angles and centroid depths of offshore earthquakes—
252 which are important for distinguishing interplate and intraslab earthquakes—were different.
253 This was clearly illustrated in detailed comparisons of seismicity southeast off the Kii
254 Peninsula and off the Hyuga-nada (Figures 6, 7, S3, and S4). The dip angles of offshore
255 earthquakes that occurred outside of onshore seismic arrays were poorly estimated by the
256 conventional 1D CMT inversion due to the lack of the subducting oceanic plate and the
257 accretionary prism (e.g. Takemura, Kimura, *et al.* 2018, Takemura, Matsuzawa, *et al.* 2018).

258 We focused our attention on seismicity southeast off the Kii Peninsula and the Hyuga-nada
259 (local names are illustrated in Figure 1), where seismic activities are relatively high in the
260 Nankai subduction zone. Figure 6 shows spatial distributions of the CMT solutions southeast
261 off the Kii Peninsula. We also plotted shallow VLFs in the catalogue of Takemura,
262 Matsuzawa, *et al.* (2019) as grey focal spheres. Shallow VLFs, which were characterised by
263 low-angle thrust faulting, were concentrated near the trench. In the region with shallow
264 VLF active, no CMT solution suggesting slip on the plate boundary was estimated. On the
265 down-dip side of the shallow VLF region, a low-angle thrust faulting mechanism was
266 estimated at a depth near the plate boundary (along profile A in Figure 6). This earthquake is
267 the 2016 southeast off the Kii Peninsula earthquake (Figure 3). Almost all of the other
268 earthquakes plotted in Figure 6 are aftershocks of the 2004 M_w 7.5 intraslab earthquake that
269 occurred on 5 September 2004 southeast off the Kii Peninsula. Our CMT solutions of these
270 aftershocks were separately distributed at depths within the oceanic crust and mantle (10–15
271 and 20–30 km depths). This separation corresponded well to the hypocentre depth
272 distributions of the aftershocks of the M_w 7.5 earthquake as determined using temporal
273 ocean-bottom seismometers (e.g. Sakai *et al.*, 2005). On the other hand, almost all the
274 centroid depths of the F-net solutions were concentrated within the crust and oceanic crust
275 (5–15 km depths; Figure S3).

276 Figure 7 shows the spatial distribution of the CMT solutions around the Hyuga-nada
277 region. Our CMT solutions characterised by low-angle thrust faulting mechanisms were
278 distributed across the region with average slip rates of approximately 20–40 mm/yr as
279 inferred from small repeating earthquakes (Igarashi 2010, Yamashita *et al.* 2012). The
280 optimal centroid depths of such thrust solutions were concentrated around the plate boundary
281 (profiles B and C in Figure 7). The dip angles of the F-net MT solutions at depths around the

282 plate boundary were slightly higher than those of the plate boundary, as shown in Figure S4.
283 This also might have been due to a lack of 3D geometry of the subducting oceanic plate in the
284 1D analysis.

285

286 **4. Discussion**

287 **4.1. Slip behaviours on the plate boundary along the Nankai Trough**

288 In order to discuss slip behaviours on the plate boundary, we selected low-angle thrust
289 faulting solutions at depths around the plate boundary from our 3D CMT catalogue. These
290 selected events could be interpreted as seismic slips on the plate boundary. Figure 8 shows
291 the spatial distribution of earthquakes with low-angle ($< 25^\circ$) thrust faulting solutions at
292 depths around the plate boundary along the Nankai Trough.

293 In Figure 8, we also plotted related seismic activity. The large coseismic slip area of the
294 1968 M_w 7.5 earthquake (Yagi *et al.* 1998) is indicated by the blue area in Figure 8. The
295 cumulative deep SSE slips in each grid were determined by summing slips of each SSE in
296 each catalogue (Nishimura *et al.* 2013, Takagi *et al.* 2016, 2019). We then evaluated the SSE
297 slip rates by dividing the cumulative SSE slip at each grid by the analysis period of each
298 catalogue. The SSE slip rate indicates the activity of deep, slow earthquakes (e.g. Ito *et al.*
299 2007, Obara & Kato 2016). We did not calculate SSE slip rates for shallow SSEs reported
300 by Yokota & Ishikawa (2019) because the number of detected events was still few at each
301 region. For similar reasons, the long-term SSEs off the Kii Channel (Kobayashi 2014) and
302 Tokai (Miyazaki *et al.* 2006) regions were also excluded from the SSE slip rate calculation.
303 Thus, we plotted the fault configurations or large slip areas of long-term SSEs and shallow
304 SSEs. We also plotted shallow LFTs (Yamashita *et al.* 2015) and shallow VLFs (Takemura,
305 Noda, *et al.* 2019) as indicators of shallow, slow earthquake activity. The spatial distribution
306 of slip-deficit rates from GNSS and GNSS-A observations by Noda *et al.* (2018), is plotted
307 using blue contour lines in Figure 8.

308 At deeper depths (30–40 km), deep slow earthquakes were active, especially in areas with
309 high SSE slip rates, but no interplate regular earthquakes were found. Although SSEs were
310 not removed in the slip-deficit rate estimation of Noda *et al.* (2018)—except for long-term
311 SSEs at the Bungo Channel—the regions with deep SSEs were characterised by low (20–40
312 mm/y) slip-deficit rates. At shallower depths (< 30 km) in the offshore region, regular
313 earthquakes, slow earthquakes, and high (> 60 mm/y) slip-deficit zones were separately
314 distributed. Similar separation of the repeating earthquakes, slow earthquakes, and large

315 coseismic slip areas of megathrust earthquakes at shallower depths were observed in the
316 regions of Tohoku (e.g. Matsuzawa *et al.* 2015, Nishikawa *et al.* 2019, Tanaka *et al.* 2019),
317 Central Ecuador (e.g. Rolandone *et al.* 2018, Vaca *et al.* 2018) and Costa Rica (e.g. Dixon *et*
318 *al.* 2014). In particular, Nishikawa *et al.* (2019) pointed out that slow earthquakes were
319 complementarily distributed in the regions surrounding the large coseismic slip area of the
320 2011 M_w 9.0 Tohoku earthquake. Takemura, Noda, *et al.* (2019) pointed out that shallow,
321 slow earthquakes cluster or migrate due to the existence of pore fluid in the transitional
322 regions between high-strength and low-strength zones of the plate boundary. According to
323 these previous studies and our observations, we suggest that the observed separation between
324 slip behaviours on the plate boundary along the Nankai Trough are related to the
325 heterogeneous distribution of effective strengths on the plate boundary, which is controlled by
326 the frictional coefficient, pore fluid pressure, and normal stress.

327

328 **4.2. Regional 3D CMT inversions for the M_w 7.2 and 7.5 earthquakes southeast off the** 329 **Kii Peninsula**

330 We conducted 3D CMT inversions of offshore earthquakes with M_w of 4.3–6.5. During
331 the analysis period (April 2004 to August 2019), M_w 7.2 and 7.5 intraslab earthquakes occurred
332 southeast off the Kii Peninsula on 5 September 2004. Because typical M_w 7 class earthquakes
333 have rupture durations of 30–50 s and fault areas of 1000–5000 km² (e.g. Kanamori & Brodsky
334 2004, Vallée & Douet 2016), precise source parameter estimation for such earthquakes is
335 difficult based on our assumptions of the CMT inversion. We, therefore, tested the CMT
336 inversion of the M_w 7.2 and 7.5 southeast off the Kii Peninsula earthquakes. Because amplitude
337 saturation of F-net broadband seismometers occurs for regional large earthquakes, we used F-
338 net strong motion seismometers, which have a large clip level and a similar frequency response
339 to STS-2 seismometers. We selected F-net stations with distances of 200–500 km from the
340 initial epicentre, which were slightly far from the original CMT settings (100–400 km).

341 Figures 9 and 10 show the results of CMT inversions for the M_w 7.2 and 7.5 earthquakes
342 southeast off the Kii Peninsula, respectively. Detailed estimated parameters are also listed in
343 Table S2. Signal-to-noise ratios were enough high compared to smaller ($M_w < 4.5$)
344 earthquakes in this study but the VRs were low compared to those of moderate earthquakes.
345 The synthetic waveforms roughly corresponded to the observed ones (Figures 9b and 10b).
346 Due to the assumptions of a point source and simple-source time function, detailed
347 characteristics of the observed waveforms were not successfully reproduced. Furthermore,
348 the high (> 66%) VR areas were wider than the CMT results for moderate earthquakes within
349 the same region (Figure 3). This suggests the likely complexity of the rupture processes and

350 the source extents for the M_w 7.2 and 7.5 earthquakes. Estimated moment magnitudes were
351 slightly smaller than those of the GCMT catalogue as a result of analysed period and the
352 deeper centroid depths.

353 We also compared our CMT result for the M_w 7.2 earthquake with the finite-fault model
354 (Okuwaki & Yagi 2018) conducted using teleseismic records based on Yagi & Fukahata
355 (2011). Our horizontal centroid location was very close to an area with a large (> 3 m)
356 coseismic slip (Figure 11). The depths of such large coseismic slips in the finite fault model
357 ranged from 9 to 18 km but the optimal centroid depth of the 3D CMT inversion was 26 km.
358 The finite fault model of Okuwaki & Yagi (2018) was conducted using teleseismic records
359 and the 1D Earth model. Although this approach provides robust solutions in earthquake
360 faulting models, depth resolutions are generally limited compared to regional analysis (e.g.
361 see Figure 4 in Koketsu *et al.* 2011). According to the hypocentre determinations derived
362 using ocean-bottom seismometers (Sakai *et al.* 2005, Nakano *et al.* 2015), the hypocentres of
363 aftershocks due to the M_w 7.5 earthquake were distributed at depths of approximately 10–30
364 km. Based on this and the fault dimensions of the M_w 7.2 earthquake, we considered that the
365 extension of seismic slips at depths of approximately 26 km might be possible.

366

367 **5. Conclusion**

368 We conducted 3D CMT inversions of moderate earthquakes along the Nankai Trough
369 using the regional 3D Green's function dataset. By introducing 3D heterogeneities, our CMT
370 method based on onshore seismograms provided better constrained focal mechanisms and
371 centroid depths compared to regional 1D analysis of the F-net MT catalogue. Although no
372 suggestive interplate earthquakes are listed in the 1D catalogue, some low-angle thrust
373 faulting solutions at depths around the plate boundary were confirmed by our 3D CMT
374 catalogue. By using our 3D CMT catalogue and previously published slow earthquake
375 models, we illustrated the spatial distribution of slip behaviours on the plate boundary along
376 the Nankai Trough. Regular interplate earthquakes and slow earthquakes were separately
377 distributed on the plate boundary. These separated distributions might reflect the
378 heterogeneous distribution of effective strength on the plate boundary. The gap zones of both
379 regular interplate and slow earthquakes were found in the Nankai, Tonankai, and Tokai
380 regions. These were the regions with large (> 60 mm/y) slip-deficit rates, where the plate
381 boundary can be strongly coupled.

382 The regional CMT inversion of earthquakes with $M_w > 7$ was generally difficult due to

383 their fault size and the amplitude saturation of the broadband sensors. CMT inversions for the
384 2004 M_w 7.2 and 7.5 intraslab earthquakes southeast of the Kii Peninsula were performed
385 using the regional broadband strong motion sensors of F-net. Although signal-to-noise ratios
386 of the observed displacements were enough good, the waveform fittings of the M_w 7.2 and
387 7.5 intraslab earthquakes were not good compared to those of typical moderate earthquakes
388 due to fault sizes and the rupture complexity. However, the estimated focal mechanisms were
389 very similar to those in the GCMT catalogue. Our grid search CMT inversion required
390 approximately 15–20 minutes to run using a single-core desktop computer. This offers
391 potential advantages for CMT-based tsunami warning systems (e.g. Reymond *et al.* 2012,
392 Miyoshi *et al.* 2015, Inazu *et al.* 2016).

393 The detailed rupture processes of the M_w 7.2 and 7.5 earthquakes remain unclear. The
394 regional seismic data and 3D Green's functions may provide additional constraints for large
395 offshore earthquakes. The finite fault modelling based on the 3D Green's functions is an
396 important but challenging issue that requires particular attention in future studies.

397

398 **Acknowledgements**

399 F-net waveform data and the F-net MT catalogue are available via the website of the National
400 Research Institute for Earth Science and Disaster Resilience
401 (<https://doi.org/10.17598/NIED.0005>). Bathymetric depth data was obtained from ETOPO1
402 (Amante & Eakins 2009). OpenSWPC software (Maeda *et al.* 2017) and the 3D model of
403 Koketsu *et al.* (2012) were obtained from <https://github.com/takuto-maeda/OpenSWPC> and
404 https://www.jishin.go.jp/evaluation/seismic_hazard_map/lpshm/12_choshuki_dat/,
405 respectively. Generic Mapping Tools (Wessel *et al.* 2013) and Seismic Analysis Code (SAC;
406 Helffrich *et al.* 2013) were used to make the figures and when conducting the signal
407 processing work, respectively. The catalogue of slow earthquakes (Nishimura *et al.* 2013,
408 Yamashita *et al.* 2015, Takagi *et al.* 2016) was downloaded from the Slow Earthquake
409 Database website (Kano *et al.* 2018; <http://www-solid.eps.s.u-tokyo.ac.jp/~sloweql/>). Our
410 CMT catalogue and CMT results of assumed source grids for each earthquake are available
411 from <https://doi.org/10.5281/zenodo.3523583>. The FDM simulations of seismic wave
412 propagation were conducted on the computer system of the Earthquake and Volcano
413 Information Center at the Earthquake Research Institute, the University of Tokyo. This study
414 was supported by the Japan Society for the Promotion of Science (JSPS) KAKENHI Grant
415 Numbers 17K14382 under the Grant-in-Aid for Young Scientists (B) and 19H04626 in
416 Scientific Research under Innovative Areas 'Science of Slow Earthquakes'.

417

418 **References**

- 419 Aki, K. & Richards, P. (2002) *Quantitative Seismology*, 2nd ed., University Science Books.
420 Retrieved from https://www.ldeo.columbia.edu/~richards/Aki_Richards.html
- 421 Amante, C. & Eakins, B.W. (2009) ETOPO1 1 arc-minute global relief model: Procedures,
422 data sources and analysis. NOAA Technical Memorandum NESDIS NGDC-24. *NOAA*
423 *Tech. Memo. NESDIS NGDC-24. Natl. Geophys. Data Center, NOAA*, 19.
424 doi:10.7289/V5C8276M
- 425 Ando, M. (1975) Source mechanisms and tectonic significance of historical earthquakes
426 along the Nankai trough, Japan. *Tectonophysics*, **27**, 119–140. doi:10.1016/0040-
427 1951(75)90102-X
- 428 Dixon, T.H., Jiang, Y., Malservisi, R., McCaffrey, R., Voss, N., Protti, M. & Gonzalez, V.
429 (2014) Earthquake and tsunami forecasts: Relation of slow slip events to subsequent
430 earthquake rupture. *Proc. Natl. Acad. Sci.*, **111**, 17039–17044.
431 doi:10.1073/pnas.1412299111
- 432 Dziewonski, A.M., Chou, T.-A. & Woodhouse, J.H. (1981) Determination of earthquake
433 source parameters from waveform data for studies of global and regional seismicity. *J.*
434 *Geophys. Res. Solid Earth*, **86**, 2825–2852. doi:10.1029/JB086iB04p02825
- 435 Eberhart-Phillips, D., Reyners, M., Bannister, S., Chadwick, M. & Ellis, S. (2010)
436 Establishing a versatile 3-D seismic velocity model for New Zealand. *Seismol. Res.*
437 *Lett.*, **81**, 992–1000. doi:10.1785/gssrl.81.6.992
- 438 Eisner, L. & Clayton, R.W. (2001) A reciprocity method for multiple-source simulations.
439 *Bull. Seismol. Soc. Am.*, **91**, 553–560. doi:10.1785/0120000222
- 440 Ekström, G., Nettles, M. & Dziewoński, A.M. (2012) The global CMT project 2004-2010:
441 Centroid-moment tensors for 13,017 earthquakes. *Phys. Earth Planet. Inter.*, **200–201**,
442 1–9. doi:10.1016/j.pepi.2012.04.002
- 443 Fukuyama, E., Ishida, M., Dreger, D.S. & Kawai, H. (1998) Automated seismic moment
444 tensor determination by using on-line broadband seismic waveforms. *Zisin*, **51**, 149–
445 156. doi:10.4294/zisin1948.51.1_149
- 446 Furumura, T., Hayakawa, T., Nakamura, M., Koketsu, K. & Baba, T. (2008) Development of
447 long-period ground motions from the Nankai trough, Japan, earthquakes: Observations
448 and computer simulation of the 1944 Tonankai (Mw 8.1) and the 2004 SE Off-Kii
449 Peninsula (Mw 7.4) earthquakes. *Pure Appl. Geophys.*, **165**, 585–607.
450 doi:10.1007/s00024-008-0318-8
- 451 Gokhberg, A. & Fichtner, A. (2016) Full-waveform inversion on heterogeneous HPC
452 systems. *Comput. Geosci.*, **89**, 260–268, Elsevier. doi:10.1016/j.cageo.2015.12.013
- 453 Gomberg, J. (2018) Cascadia Onshore-Offshore Site Response, Submarine Sediment
454 Mobilization, and Earthquake Recurrence. *J. Geophys. Res. Solid Earth*.
455 doi:10.1002/2017JB014985
- 456 Guo, Y., Koketsu, K. & Miyake, H. (2016) Propagation mechanism of long-period ground

- 457 motions for offshore earthquakes along the Nankai trough: Effects of the accretionary
458 wedge. *Bull. Seismol. Soc. Am.*, **106**, 1176–1197. doi:10.1785/0120150315
- 459 Hardebeck, J.L. & Shearer, P.M. (2002) A new method for determining first-motion focal
460 mechanisms. *Bull. Seismol. Soc. Am.*, **92**, 2264–2276. doi:10.1785/0120010200
- 461 Hejrani, B., Tkalčić, H. & Fichtner, A. (2017) Centroid moment tensor catalogue using a 3-D
462 continental scale Earth model: Application to earthquakes in Papua New Guinea and the
463 Solomon Islands. *J. Geophys. Res. Solid Earth*, **122**, 5517–5543.
464 doi:10.1002/2017JB014230
- 465 Helffrich, G., Wookey, J. & Bastow, I. (2013) *The Seismic Analysis Code*, Cambridge:
466 Cambridge University Press. doi:10.1017/CBO9781139547260
- 467 Igarashi, T. (2010) Spatial changes of inter-plate coupling inferred from sequences of small
468 repeating earthquakes in Japan. *Geophys. Res. Lett.*, **37**, 1–5.
469 doi:10.1029/2010GL044609
- 470 Inazu, D., Pulido, N., Fukuyama, E., Saito, T., Senda, J. & Kumagai, H. (2016) Near-field
471 tsunami forecast system based on near real-time seismic moment tensor estimation in the
472 regions of Indonesia, the Philippines, and Chile 4. *Seismology. Earth, Planets Sp.*, **68**,
473 Springer Berlin Heidelberg. doi:10.1186/s40623-016-0445-x
- 474 Ito, Y. & Obara, K. (2006) Dynamic deformation of the accretionary prism excites very low
475 frequency earthquakes. *Geophys. Res. Lett.*, **33**, L02311. doi:10.1029/2005GL025270
- 476 Ito, Y., Obara, K., Shiomi, K., Sekine, S. & Hirose, H. (2007) Slow earthquakes coincident
477 with episodic tremors and slow slip events. *Science (80-.)*, **315**, 503–506.
478 doi:10.1126/science.1134454
- 479 Iwaki, A., Maeda, T., Morikawa, N., Takemura, S. & Fujiwara, H. (2018) Effects of random
480 3D upper crustal heterogeneity on long-period (≥ 1 s) ground-motion simulations. *Earth,*
481 *Planets Sp.*, **70**, 156. doi:10.1186/s40623-018-0930-5
- 482 Kamei, R., Pratt, R.G. & Tsuji, T. (2012) Waveform tomography imaging of a megasplay
483 fault system in the seismogenic Nankai subduction zone. *Earth Planet. Sci. Lett.*, **317–**
484 **318**, 343–353, Elsevier B.V. doi:10.1016/j.epsl.2011.10.042
- 485 Kanamori, H. & Brodsky, E.E. (2004) The physics of earthquakes. *Reports Prog. Phys.*, **67**,
486 1429–1496. doi:10.1088/0034-4885/67/8/R03
- 487 Kanamori, H. & Rivera, L. (2008) Source inversion of W phase: Speeding up seismic
488 tsunami warning. *Geophys. J. Int.*, **175**, 222–238. doi:10.1111/j.1365-
489 246X.2008.03887.x
- 490 Kaneko, Y., Ito, Y., Chow, B., Wallace, L.M., Grapenthin, R., Anastasio, E.D. & Henrys, S.
491 (2019) Ultra-long duration of seismic ground motion arising from a thick, low velocity
492 sedimentary wedge. *J. Geophys. Res. Solid Earth*, **124**. doi:10.1029/2019JB017795
- 493 Kano, M., Aso, N., Matsuzawa, T., Ide, S., Annoura, S., Arai, R., Baba, S., *et al.* (2018)
494 Development of a Slow Earthquake Database, **89**, 1566–1575. doi:10.1785/0220180021

- 495 Kikuchi, M. & Kanamori, H. (1991) Inversion of complex body waves-III. *Bull. Seism. Soc.*
496 *Am.*, **81**, 2335–2350. Retrieved from
497 [https://pubs.geoscienceworld.org/ssa/bssa/article/81/6/2335/102472/inversion-of-](https://pubs.geoscienceworld.org/ssa/bssa/article/81/6/2335/102472/inversion-of-complex-body-waves-iii)
498 [complex-body-waves-iii](https://pubs.geoscienceworld.org/ssa/bssa/article/81/6/2335/102472/inversion-of-complex-body-waves-iii)
- 499 Kimura, T., Murakami, H. & Matsumoto, T. (2015) Systematic monitoring of instrumentation
500 health in high-density broadband seismic networks. *Earth, Planets Sp.*, **67**, ???
501 doi:10.1186/s40623-015-0226-y
- 502 Kobayashi, A. (2014) A long-term slow slip event from 1996 to 1997 in the Kii Channel,
503 Japan. *Earth, Planets Sp.*, **66**, 1–7. doi:10.1186/1880-5981-66-9
- 504 Koketsu, K., Miyake, H. & Suzuki, H. (2012) Japan Integrated Velocity Structure Model
505 Version 1. *Proc. 15th World Conf. Earthq. Eng.*, 1–4. Retrieved from
506 http://www.iitk.ac.in/nicee/wcee/article/WCEE2012_1773.pdf
- 507 Koketsu, K., Yokota, Y., Nishimura, N., Yagi, Y., Miyazaki, S., Satake, K., Fujii, Y., *et al.*
508 (2011) A unified source model for the 2011 Tohoku earthquake. *Earth Planet. Sci. Lett.*,
509 **310**, 480–487. doi:10.1016/j.epsl.2011.09.009
- 510 Kubo, A., Fukuyama, E., Kawai, H. & Nonomura, K. (2002) NIED seismic moment tensor
511 catalogue for regional earthquakes around Japan: Quality test and application.
512 *Tectonophysics*, **356**, 23–48. doi:10.1016/S0040-1951(02)00375-X
- 513 Kubota, T., Suzuki, W., Nakamura, T., Chikasada, N.Y., Aoi, S., Takahashi, N. & Hino, R.
514 (2018) Tsunami source inversion using time-derivative waveform of offshore pressure
515 records to reduce effects of non-tsunami components. *Geophys. J. Int.*, **215**, 1200–1214,
516 Oxford University Press. doi:10.1093/GJI/GGY345
- 517 Lee, S.-J., Liang, W.T., Cheng, H.W., Tu, F.S., Ma, K.F., Tsuruoka, H., Kawakatsu, H., *et al.*
518 (2013) Towards real-time regional earthquake simulation I: Real-time moment tensor
519 monitoring (RMT) for regional events in Taiwan. *Geophys. J. Int.*, **196**, 432–446.
520 doi:10.1093/gji/ggt371
- 521 Lee, S.-J., Liu, Q., Tromp, J., Komatitsch, D., Liang, W.T. & Huang, B.S. (2014) Toward
522 real-time regional earthquake simulation II: Real-time Online earthquake Simulation
523 (ROS) of Taiwan earthquakes. *J. Asian Earth Sci.*, **87**, 56–68, Elsevier Ltd.
524 doi:10.1016/j.jseaes.2014.02.009
- 525 Maeda, T., Takemura, S. & Furumura, T. (2017) OpenSWPC: an open-source integrated
526 parallel simulation code for modeling seismic wave propagation in 3D heterogeneous
527 viscoelastic media. *Earth, Planets Sp.*, **69**, 102, Springer Berlin Heidelberg.
528 doi:10.1186/s40623-017-0687-2
- 529 Matsuzawa, T., Asano, Y. & Obara, K. (2015) Very low frequency earthquakes off the
530 Pacific coast of Tohoku, Japan. *Geophys. Res. Lett.*, **42**, 4318–4325.
531 doi:10.1002/2015GL063959
- 532 Miyazaki, S., Segall, P., McGuire, J.J., Kato, T. & Hatanaka, Y. (2006) Spatial and temporal

- 533 evolution of stress and slip rate during the 2000 Tokai slow earthquake. *J. Geophys. Res.*
534 *Solid Earth*, **111**, 1–17. doi:10.1029/2004JB003426
- 535 Miyazawa, M. (2019) Bayesian approach for detecting dynamically triggered very low-
536 frequency earthquakes in the Nankai subduction zone and application to the 2016 M w
537 5.9 off-Kii Peninsula earthquake, Japan. *Geophys. J. Int.*, **217**, 1123–1140, Oxford
538 University Press. doi:10.1093/gji/ggz073
- 539 Miyoshi, T., Saito, T., Inazu, D. & Tanaka, S. (2015) Tsunami modeling from the seismic
540 CMT solution considering the dispersive effect: A case of the 2013 Santa Cruz Islands
541 tsunami 4. *Seismology. Earth, Planets Sp.*, **67**. doi:10.1186/s40623-014-0179-6
- 542 Nakajima, J. & Hasegawa, A. (2007) Subduction of the Philippine Sea plate beneath
543 southwestern Japan: Slab geometry and its relationship to arc magmatism. *J. Geophys.*
544 *Res. Solid Earth*, **112**, 1–18. doi:10.1029/2006JB004770
- 545 Nakamura, T., Takenaka, H., Okamoto, T., Ohori, M. & Tsuboi, S. (2015) Long-period
546 ocean-bottom motions in the source areas of large subduction earthquakes. *Sci. Rep.*, **5**,
547 1–2. doi:10.1038/srep16648
- 548 Nakano, M., Hori, T., Araki, E., Kodaira, S. & Ide, S. (2018) Shallow very-low-frequency
549 earthquakes accompany slow slip events in the Nankai subduction zone. *Nat. Commun.*,
550 **9**, 984. doi:10.1038/s41467-018-03431-5
- 551 Nakano, M., Hyodo, M., Nakanishi, A., Yamashita, M., Hori, T., Kamiya, S. ichiro, Suzuki,
552 K., *et al.* (2018) The 2016 Mw5.9 earthquake off the southeastern coast of Mie
553 Prefecture as an indicator of preparatory processes of the next Nankai Trough
554 megathrust earthquake. *Prog. Earth Planet. Sci.*, **5**, Progress in Earth and Planetary
555 Science. doi:10.1186/s40645-018-0188-3
- 556 Nakano, M., Nakamura, T. & Kaneda, Y. (2015) Hypocenters in the nankai trough
557 determined by using data from both ocean-bottom and land seismic networks and a 3D
558 velocity structure model: Implications for seismotectonic activity. *Bull. Seismol. Soc.*
559 *Am.*, **105**, 1594–1605. doi:10.1785/0120140309
- 560 National Research Institute for Earth Science and Disaster Resilience. (2019) NIED F-net.
561 *Natl. Res. Inst. Earth Sci. Disaster Resil.*, National Research Institute for Earth Science
562 and Disaster Resilience. doi:10.17598/NIED.0005
- 563 Nishida, K., Kawakatsu, H. & Obara, K. (2008) Three-dimensional crustal S wave velocity
564 structure in Japan using microseismic data recorded by Hi-net tiltmeters. *J. Geophys.*
565 *Res. Solid Earth*, **113**, 1–22. doi:10.1029/2007JB005395
- 566 Nishikawa, T., Matsuzawa, T., Ohta, K., Uchida, N., Nishimura, T. & Ide, S. (2019) The
567 slow earthquake spectrum in the Japan Trench illuminated by the S-net seafloor
568 observatories. *Science (80-.)*, **365**, 808–813. doi:10.1126/science.aax5618
- 569 Nishimura, T., Matsuzawa, T. & Obara, K. (2013) Detection of short-term slow slip events
570 along the Nankai Trough, southwest Japan, using GNSS data. *J. Geophys. Res. Solid*

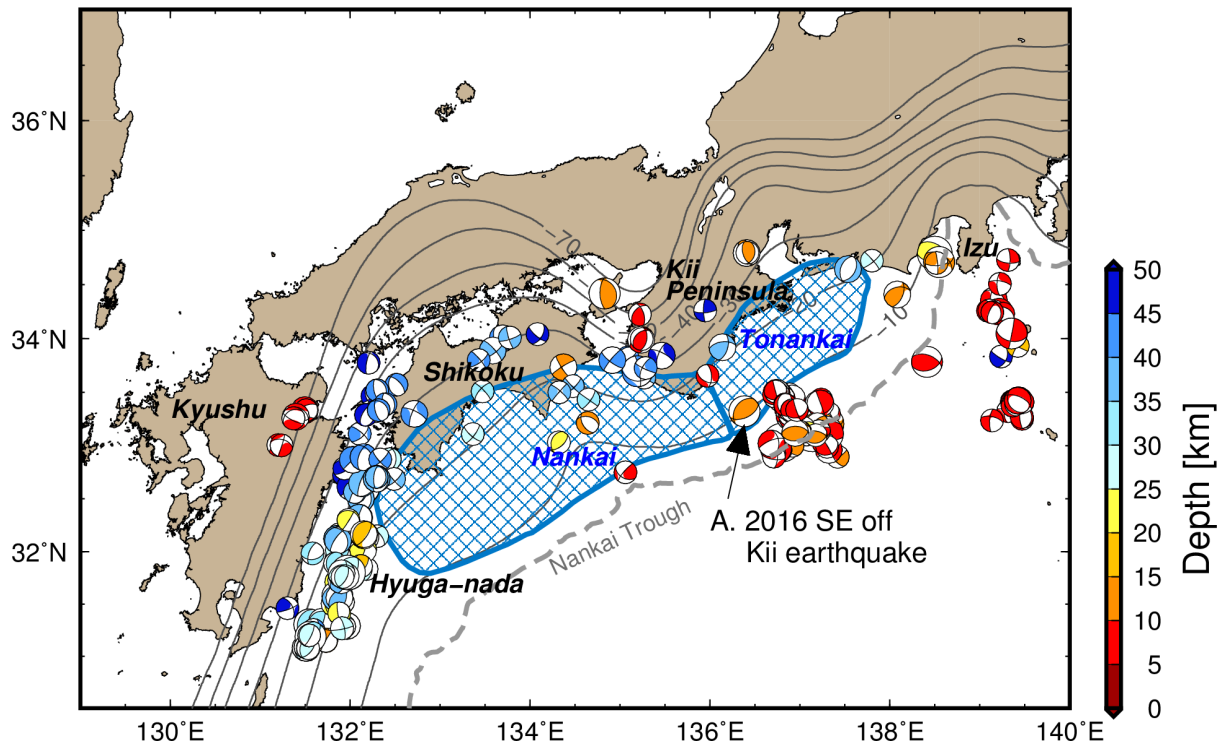
- 571 *Earth*, **118**, 3112–3125, Wiley-Blackwell. doi:10.1002/jgrb.50222
- 572 Noda, A., Saito, T. & Fukuyama, E. (2018) Slip-deficit rate distribution along the Nankai
573 trough, southwest Japan, with elastic lithosphere and viscoelastic asthenosphere. *J.*
574 *Geophys. Res. Solid Earth*, **123**, 8125–8142. doi:10.1029/2018JB015515
- 575 Obara, K. & Kato, A. (2016) Connecting slow earthquakes to huge earthquakes. *Science*
576 (80-), **353**, 253–257. doi:10.1126/science.aaf1512
- 577 Okada, Y., Kasahara, K., Hori, S., Obara, K., Sekiguchi, S., Fujiwara, H. & Yamamoto, A.
578 (2004) Recent progress of seismic observation networks in Japan —Hi-net, F-net, K-
579 NET and KiK-net—. *Earth, Planets Sp.*, **56**, xv–xxviii. doi:10.1186/BF03353076
- 580 Okamoto, T., Takenaka, H. & Nakamura, T. (2018) Evaluation of accuracy of synthetic
581 waveforms for subduction-zone earthquakes by using a land–ocean unified 3D structure
582 model. *Earth, Planets Sp.*, **70**, Springer Berlin Heidelberg. doi:10.1186/s40623-018-
583 0871-z
- 584 Okuwaki, R. & Yagi, Y. (2018) Seismic source model for the Mw 7.2 2004 Kii peninsula,
585 Japan, earthquake. *Github*. doi:10.5281/zenodo.1493833
- 586 Park, J.-O., Fujie, G., Wijerathne, L., Hori, T., Kodaira, S., Fukao, Y., Moore, G.F., *et al.*
587 (2010) A low-velocity zone with weak reflectivity along the Nankai subduction zone.
588 *Geology*, **38**, 283–286. doi:10.1130/G30205.1
- 589 Park, S. & Ishii, M. (2018) Near-surface compressional and shear wave speeds constrained
590 by body-wave polarization analysis. *Geophys. J. Int.*, **213**, 1559–1571.
591 doi:10.1093/gji/ggy072
- 592 Petukhin, A., Miyakoshi, K., Tsurugi, M., Kawase, H. & Kamae, K. (2016) Visualization of
593 Green’s function anomalies for megathrust source in Nankai Trough by reciprocity
594 method. *Earth, Planets Sp.*, **68**, Earth, Planets and Space. doi:10.1186/s40623-016-
595 0385-5
- 596 Ramos-Martínez, J. & McMechan, G.A. (2001) Source-parameter estimation by full
597 waveform inversion in 3D heterogeneous, viscoelastic, anisotropic media. *Bull. Seismol.*
598 *Soc. Am.*, **91**, 276–291. doi:10.1785/0120000017
- 599 Reymond, D., Okal, E.A., Hébert, H. & Bourdet, M. (2012) Rapid forecast of tsunami wave
600 heights from a database of pre-computed simulations, and application during the 2011
601 Tohoku tsunami in French Polynesia. *Geophys. Res. Lett.*, **39**, 1–6.
602 doi:10.1029/2012GL051640
- 603 Rolandone, F., Nocquet, J.M., Mothes, P.A., Jarrin, P., Vallée, M., Cubas, N., Hernandez, S.,
604 *et al.* (2018) Areas prone to slow slip events impede earthquake rupture propagation and
605 promote afterslip. *Sci. Adv.*, **4**, 2–10. doi:10.1126/sciadv.aao6596
- 606 Saito, T., Noda, A., Yoshida, K. & Tanaka, S. (2018) Shear strain energy change caused by
607 the interplate coupling along the Nankai Trough: An integration analysis using stress
608 tensor inversion and slip deficit inversion. *J. Geophys. Res. Solid Earth*.

- 609 doi:10.1029/2018JB015839
- 610 Sakai, S., Yamada, T., Shinohara, M., Hagiwara, H., Kanazawa, T., Obana, K., Kodaira, S.,
611 *et al.* (2005) Urgent aftershock observation of the 2004 off the Kii Peninsula earthquake
612 using ocean bottom seismometers. *Earth Planets Sp.*, **57**, 363–368.
613 doi:10.1186/BF03352577
- 614 Shapiro, N.M., Campillo, M., Singh, S.K. & Pacheco, J. (1998) Seismic channel waves in the
615 accretionary prism of the Middle America Trench. *Geophys. Res. Lett.*, **25**, 101–104.
616 doi:10.1029/97GL03492
- 617 Shelly, D.R., Hardebeck, J.L., Ellsworth, W.L. & Hill, D.P. (2016) A new strategy for
618 earthquake focal mechanisms using waveform-correlation-derived relative polarities and
619 cluster analysis: Application to the 2014 Long Valley Caldera earthquake swarm. *J.*
620 *Geophys. Res. Solid Earth*, **121**, 8622–8641. doi:10.1002/2016JB013437
- 621 Storchak, D.A., Giacomo, D. Di, Bondár, I., Engdahl, E.R., Harris, J., Lee, W.H.K. &
622 Villaseñor, A. (2013) Public Release of the ISC – GEM Global Instrumental Earthquake
623 Catalogue (1900 – 2009). doi:10.1785/0220130034
- 624 Sugioka, H., Okamoto, T., Nakamura, T., Ishihara, Y., Ito, A., Obana, K., Kinoshita, M., *et*
625 *al.* (2012) Tsunamigenic potential of the shallow subduction plate boundary inferred
626 from slow seismic slip. *Nat. Geosci.*, **5**, 414–418, Nature Publishing Group.
627 doi:10.1038/ngeo1466
- 628 Takagi, R., Obara, K. & Maeda, T. (2016) Slow slip event within a gap between tremor and
629 locked zones in the Nankai subduction zone. *Geophys. Res. Lett.*, **43**, 1066–1074.
630 doi:10.1002/2015GL066987
- 631 Takagi, R., Uchida, N. & Obara, K. (2019) Along-Strike Variation and Migration of Long-
632 Term Slow Slip Events in the Western Nankai Subduction Zone, Japan. *J. Geophys. Res.*
633 *Solid Earth*, **124**, 3853–3880. doi:10.1029/2018JB016738
- 634 Takemura, S., Kimura, T., Saito, T., Kubo, H. & Shiomi, K. (2018) Moment tensor inversion
635 of the 2016 southeast offshore Mie earthquake in the Tonankai region using a three-
636 dimensional velocity structure model: effects of the accretionary prism and subducting
637 oceanic plate. *Earth, Planets Sp.*, **70**, 50, Springer Berlin Heidelberg.
638 doi:10.1186/s40623-018-0819-3
- 639 Takemura, S., Kobayashi, M. & Yoshimoto, K. (2017) High-frequency seismic wave
640 propagation within the heterogeneous crust: Effects of seismic scattering and intrinsic
641 attenuation on ground motion modelling. *Geophys. J. Int.*, **210**, 1806–1822.
642 doi:10.1093/gji/ggx269
- 643 Takemura, S., Kubo, H., Tonegawa, T., Saito, T. & Shiomi, K. (2019) Modeling of Long-
644 Period Ground Motions in the Nankai Subduction Zone: Model Simulation Using the
645 Accretionary Prism Derived from Oceanfloor Local S-Wave Velocity Structures. *Pure*
646 *Appl. Geophys.*, **176**, 627–647, Birkhauser Verlag AG. doi:10.1007/s00024-018-2013-8

- 647 Takemura, S., Matsuzawa, T., Kimura, T., Tonegawa, T. & Shiomi, K. (2018) Centroid
648 Moment Tensor Inversion of Shallow Very Low Frequency Earthquakes Off the Kii
649 Peninsula, Japan, Using a Three-Dimensional Velocity Structure Model. *Geophys. Res.
650 Lett.*, **45**, 6450–6458, Wiley-Blackwell. doi:10.1029/2018GL078455
- 651 Takemura, S., Matsuzawa, T., Noda, A., Tonegawa, T., Asano, Y., Kimura, T. & Shiomi, K.
652 (2019) Structural Characteristics of the Nankai Trough Shallow Plate Boundary Inferred
653 From Shallow Very Low Frequency Earthquakes. *Geophys. Res. Lett.*, **46**, 4192–4201,
654 Blackwell Publishing Ltd. doi:10.1029/2019GL082448
- 655 Takemura, S., Noda, A., Kubota, T., Asano, Y., Matsuzawa, T. & Shiomi, K. (2019)
656 Migrations and Clusters of Shallow Very Low Frequency Earthquakes in the Regions
657 Surrounding Shear Stress Accumulation Peaks along the Nankai Trough. *Geophys. Res.
658 Lett.*, 2019GL084666. doi:10.1029/2019GL084666
- 659 Takemura, S., Shiomi, K., Kimura, T. & Saito, T. (2016) Systematic difference between first
660 - motion and waveform - inversion solutions for shallow offshore earthquakes due to a
661 low - angle dipping slab. *Earth, Planets Sp.*, 1–8, Springer Berlin Heidelberg.
662 doi:10.1186/s40623-016-0527-9
- 663 Tanaka, S., Matsuzawa, T. & Asano, Y. (2019) Shallow Low-Frequency Tremor in the
664 Northern Japan Trench Subduction Zone. *Geophys. Res. Lett.*, **46**, 5217–5224.
665 doi:10.1029/2019GL082817
- 666 Terakawa, T. & Matsu'ura, M. (2010) The 3-D tectonic stress fields in and around Japan
667 inverted from centroid moment tensor data of seismic events. *Tectonics*, **29**, 1–14.
668 doi:10.1029/2009TC002626
- 669 Thurber, C., Zhang, H., Waldhauser, F., Hardebeck, J., Michael, A. & Eberhart-Phillips, D.
670 (2006) Three-dimensional compressional wavespeed model, earthquake relocations, and
671 focal mechanisms for the Parkfield, California, region. *Bull. Seismol. Soc. Am.*, **96**, 38–
672 49. doi:10.1785/0120050825
- 673 Townend, J. & Zoback, M.D. (2006) Stress, strain, and mountain building in central Japan. *J.
674 Geophys. Res. Solid Earth*, **111**, 1–11. doi:10.1029/2005JB003759
- 675 Tsuruoka, H., Kawakatsu, H. & Urabe, T. (2009) GRiD MT (grid-based real-time
676 determination of moment tensors) monitoring the long-period seismic wavefield. *Phys.
677 Earth Planet. Inter.*, **175**, 8–16. doi:10.1016/j.pepi.2008.02.014
- 678 Vaca, S., Vallée, M., Nocquet, J.M., Battaglia, J. & Régnier, M. (2018) Recurrent slow slip
679 events as a barrier to the northward rupture propagation of the 2016 Pedernales
680 earthquake (Central Ecuador). *Tectonophysics*, **724–725**, 80–92, Elsevier.
681 doi:10.1016/j.tecto.2017.12.012
- 682 Vallée, M., Charléty, J., Ferreira, A.M.G., Delouis, B. & Vergoz, J. (2011) SCARDEC: A
683 new technique for the rapid determination of seismic moment magnitude, focal
684 mechanism and source time functions for large earthquakes using body-wave

- 685 deconvolution. *Geophys. J. Int.*, **184**, 338–358. doi:10.1111/j.1365-246X.2010.04836.x
- 686 Vallée, M. & Douet, V. (2016) A new database of source time functions (STFs) extracted
687 from the SCARDEC method, **257**, 149–157. doi:10.1016/j.pepi.2016.05.012
- 688 Volk, O., Shani-kadmiel, S., Gvirtzman, Z. & Tsesarsky, M. (2017) 3D Effects of
689 Sedimentary Wedges and Subsurface Canyons : Ground-Motion Amplification in the
690 Israeli Coastal Plain, **107**. doi:10.1785/0120160349
- 691 Wallace, L.M., Araki, E., Saffer, D., Wang, X., Roesner, A., Kopf, A., Nakanishi, A., *et al.*
692 (2016) Near-field observations of an offshore M w 6.0 earthquake from an integrated
693 seafloor and subseafloor monitoring network at the Nankai Trough, southwest Japan. *J.*
694 *Geophys. Res. Solid Earth*, **121**, 8338–8351. doi:10.1002/2016JB013417
- 695 Wang, X. & Zhan, Z. (2019) Moving from 1D to 3D velocity model : automated waveform-
696 based earthquake moment tensor inversion in the Los Angeles region. *Geophys. J. Int.*
697 doi:10.1093/gji/ggz435
- 698 Wessel, P., Smith, W.H.F., Scharroo, R., Luis, J. & Wobbe, F. (2013) Generic mapping tools:
699 Improved version released. *Eos (Washington. DC).*, **94**, 409–410.
700 doi:10.1002/2013EO450001
- 701 Yagi, Y. & Fukahata, Y. (2011) Introduction of uncertainty of Green’s function into
702 waveform inversion for seismic source processes. *Geophys. J. Int.*, **186**, 711–720.
703 doi:10.1111/j.1365-246X.2011.05043.x
- 704 Yagi, Y., Kikuchi, M., Yoshida, S. & Yamanaka, Y. (1998) Source Process of the Hyuga-
705 nada Earthquake of April 1, 1968 (MJMA 7.5), and its Relationship to the Subsequent
706 Seismicity. *Zisin (Journal Seismol. Soc. Japan. 2nd ser.)*, **51**, 139–148.
707 doi:10.4294/zisin1948.51.1_139
- 708 Yamashita, Y., Shimizu, H. & Goto, K. (2012) Small repeating earthquake activity, interplate
709 quasi-static slip, and interplate coupling in the Hyuga-nada, southwestern Japan
710 subduction zone. *Geophys. Res. Lett.*, **39**, 1–5. doi:10.1029/2012GL051476
- 711 Yamashita, Y., Yakiwara, H., Asano, Y., Shimizu, H., Uchida, K., Hirano, S., Umakoshi, K.,
712 *et al.* (2015) Migrating tremor off southern Kyushu as evidence for slow slip of a
713 shallow subduction interface. *Science (80-.)*, **348**, 676–679.
714 doi:10.1126/science.aaa4242
- 715 Yokota, Y. & Ishikawa. (2019) Shallow long-term slow slip events along the Nankai Trough
716 detected by the GNSS-A. *EarthArXiv*. doi:10.31223/osf.io/vq6ca
- 717
- 718

719 **Figures**

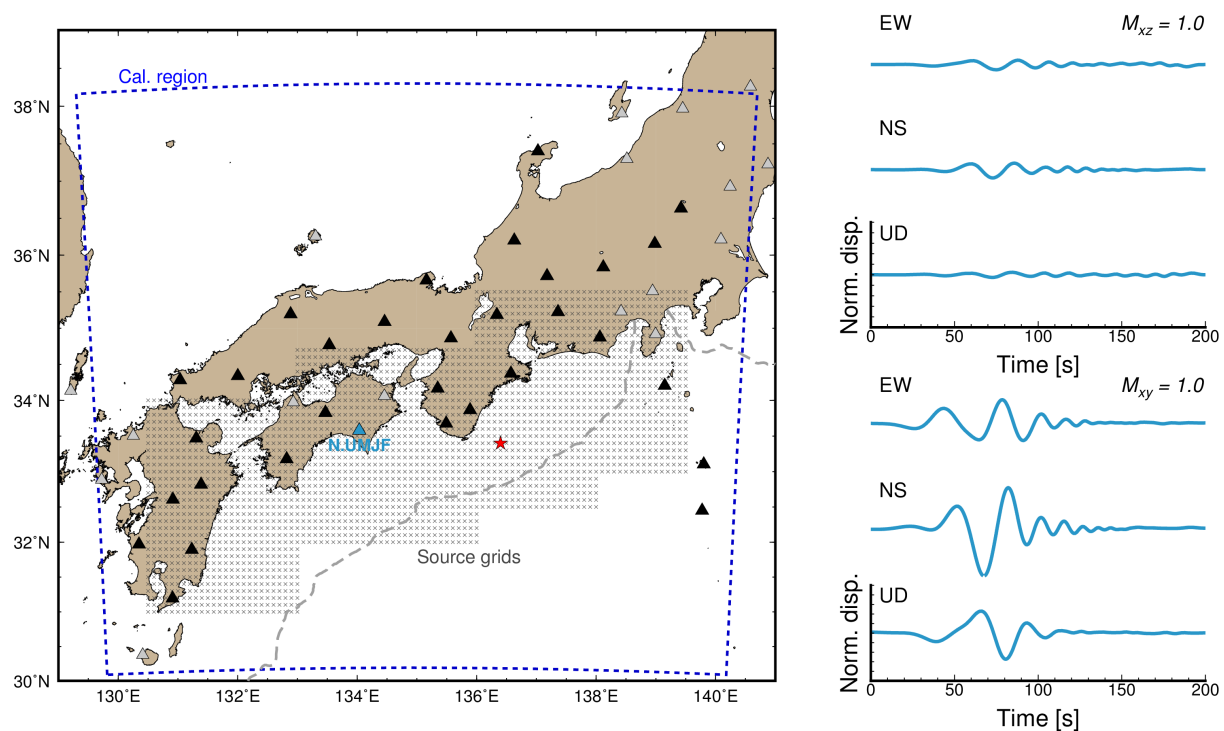


720

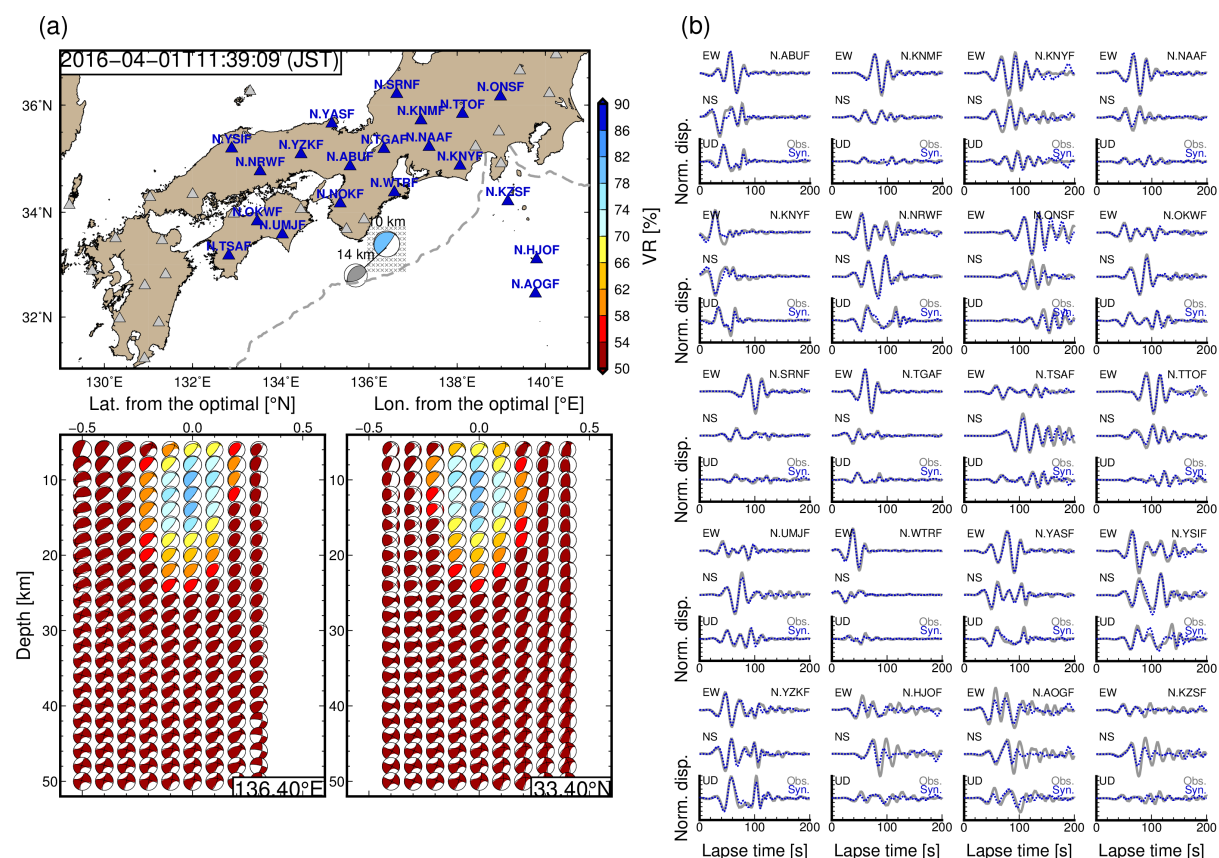
721 Figure 1. Map of the study region. The black contour lines are the iso-depth contour lines of
722 the upper surface of the Philippine Sea Plate of Koketsu *et al.* (2012). Focal mechanisms
723 are the moment tensor (MT) solutions of regular earthquakes with M_w of 4.3–6.5 in the
724 F-net catalogue (Fukuyama *et al.* 1998, Kubo *et al.* 2002) that occurred in the area with
725 latitudes less than 34.8°N, longitudes greater than 130.5°E, and at depths of less than 50
726 km. The periods of plotted MT solutions range from April 2004 to August 2019. The blue
727 hatched areas represent the expected source region of the Nankai and Tonankai
728 earthquakes (Earthquake Research Committee, 2001, available at:
729 http://www.jishin.go.jp/main/chousa/01sep_nankai/index.htm). The earthquake marked A
730 is the M_w 5.8 southeast off Kii Peninsula earthquake that occurred on 1 April 2016.

731

732



733
734 Figure 2. Calculation settings used in the study were the blue dashed line represents the
735 horizontal coverage of the simulation model region. The triangles and crosses in the map
736 denote the locations of the F-net stations and the assumed source grids, respectively.
737 Green's functions from the source grids to the black-fill and blue-fill triangles were
738 evaluated via reciprocal calculations using OpenSWPC code (Maeda *et al.* 2017). The
739 right-hand panels show examples of filtered displacements of Green's functions from a
740 certain hypocentre (red star) to the N.UMJF station (blue triangle). The filter passed band
741 ranged from 25 to 100 s.
742
743



744

745 Figure 3. CMT results for the southeast off Kii Peninsula earthquake that occurred on 1 April

746 2016. (a) Locations of the optimal solutions, used stations, and depth variations of

747 optimal solutions at each source grid. Colours of the focal mechanisms reflect values of

748 variance reduction between observed and synthetic displacements for 25–100 s periods.

749 The numbers above the optimal solutions in (a) are the optimal centroid depths. The grey

750 focal mechanism in (a) is the F-net MT solution of this earthquake. (b) Comparisons of

751 observed and synthetic displacements for 25–100 s periods. Grey solid and blue dotted

752 lines are the observed and synthetic seismograms, respectively. Synthetic seismograms

753 were evaluated by assuming the optimal solution. Amplitudes of both observed and

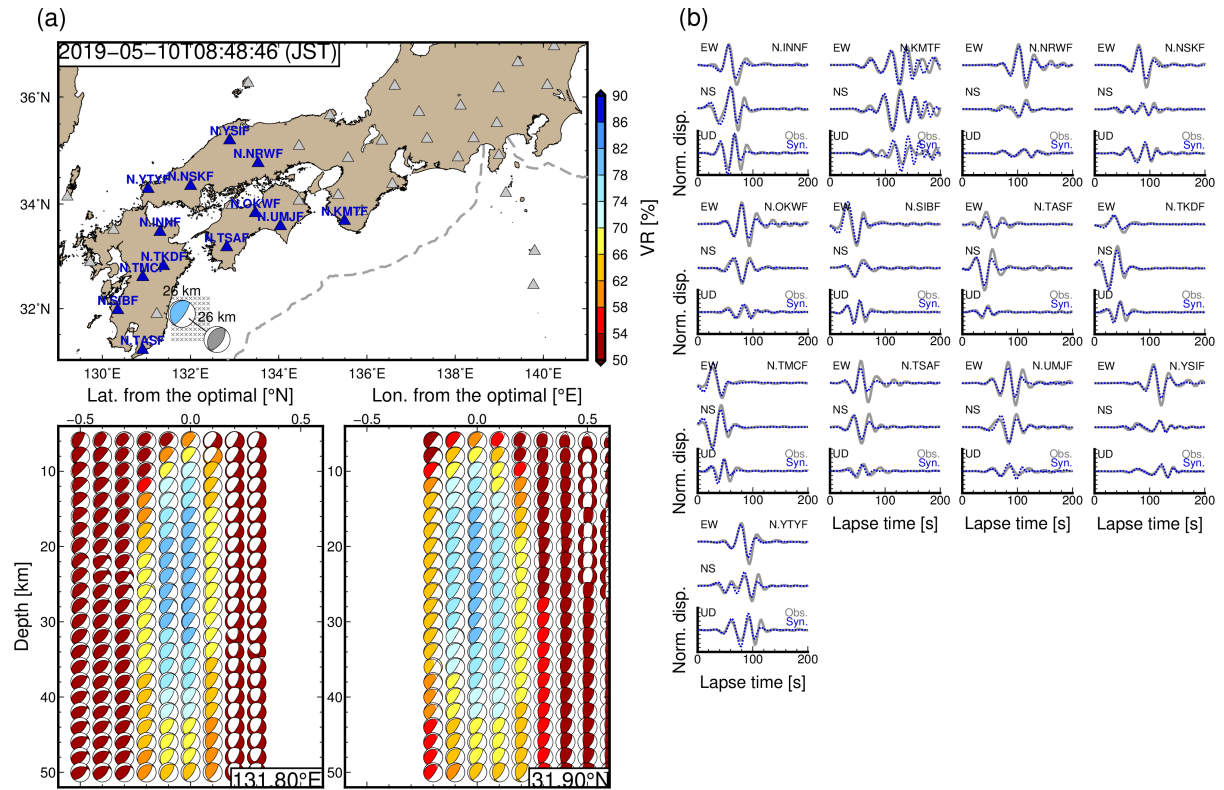
754 synthetic seismograms at each station were normalised by the maximum amplitude of the

755 observed and synthetic filtered displacements. Detailed source parameters are listed in

756 Table S1.

757

758



759

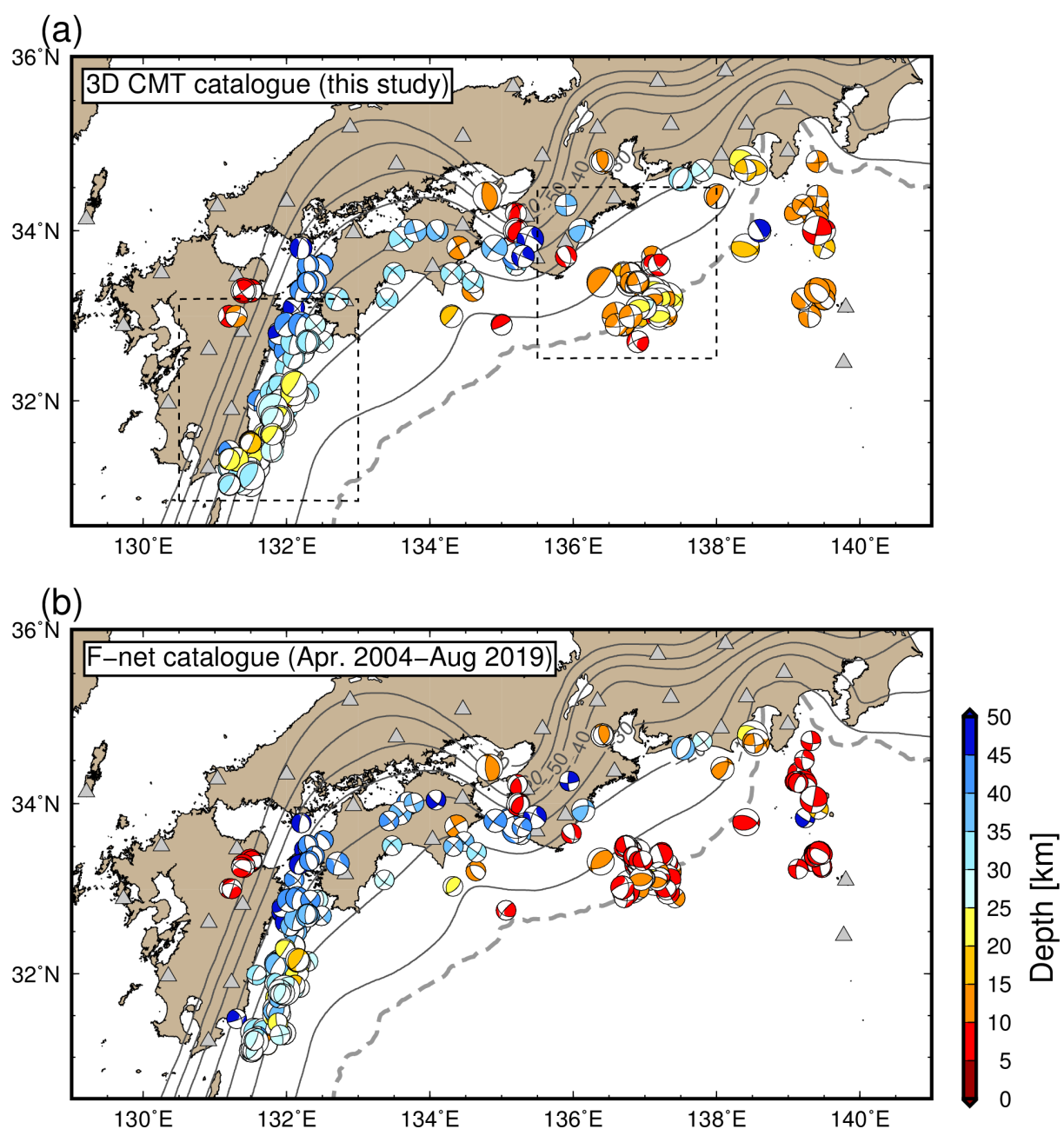
760 Figure 4. CMT results for the Hyuga-nada earthquake that occurred on 10 May 2019. (a)

761 Locations of the optimal solutions, used stations, and depth variations of optimal
 762 solutions at each source grid. Colours of the focal mechanisms reflect values of variance
 763 reduction between observed and synthetic displacements for 25–100 s periods. The
 764 numbers above the optimal solutions in (a) are the optimal centroid depths. The grey
 765 focal mechanism in (a) is the F-net MT solution of this earthquake. (b) Comparisons of
 766 observed and synthetic displacements for 25–100 s periods. Grey solid and blue dotted
 767 lines are the observed and synthetic seismograms, respectively. Synthetic seismograms
 768 were evaluated by assuming the optimal solution. Amplitudes of both observed and
 769 synthetic seismograms at each station were normalised by the maximum amplitude of the
 770 observed and synthetic filtered displacements. Detailed source parameters are listed in
 771 Table S1.

772

773

774



775

776 Figure 5. Comparisons of estimated CMT solutions between the (a) 3D CMT and (b) F-net

777 MT catalogues. Colours of focal mechanisms represent the centroid depths of each

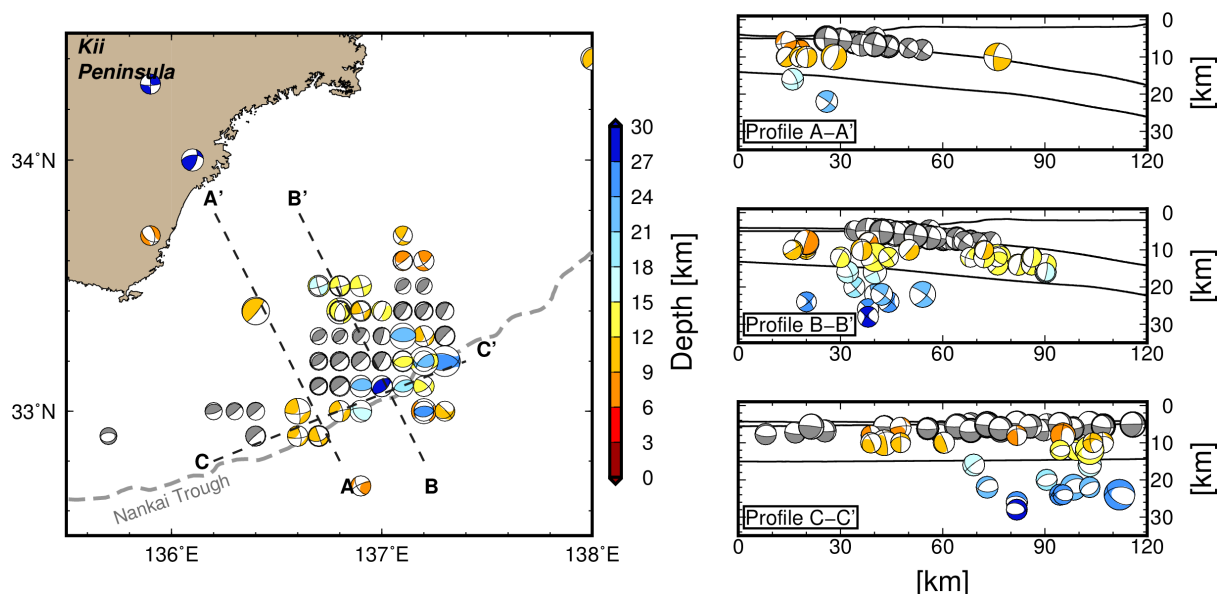
778 solution. Detailed source parameters of our 3D CMT solutions are listed in Table S1. The

779 regions enclosed by the dashed lines in (a) are enlarged in Figures 6 and 7.

780

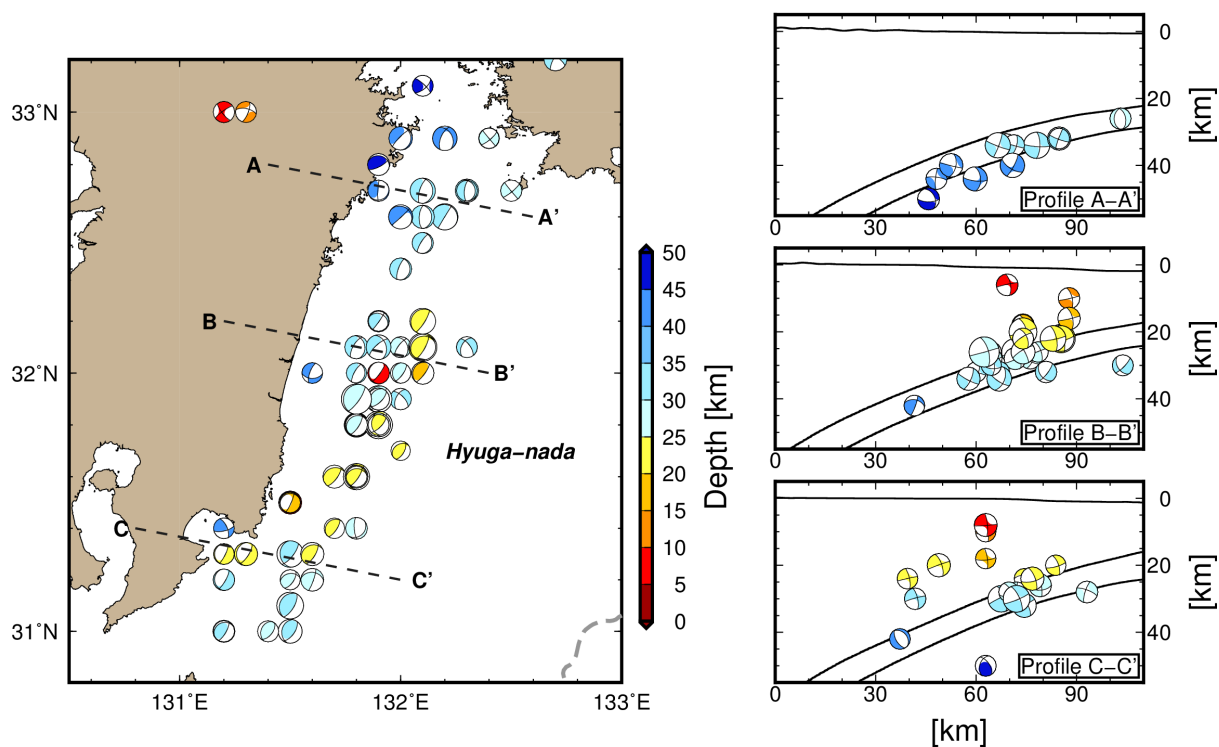
781

782



783

784 Figure 6. Spatial distribution of the CMT solutions southeast of the Kii Peninsula. Coloured
 785 focal mechanisms are our CMT solutions. Grey focal mechanisms are the CMT solutions
 786 of shallow VLFs (Takemura, Matsuzawa, *et al.* 2019). The right-hand panels show
 787 cross-sections along profiles A-A', B-B' and C-C'. The bathymetry of ETOPO1 (Amante
 788 & Eakins 2009), the upper surface, and oceanic Moho of the Philippine Sea Plate
 789 (Koketsu *et al.* 2012) along each profile are plotted in the right-hand panels.

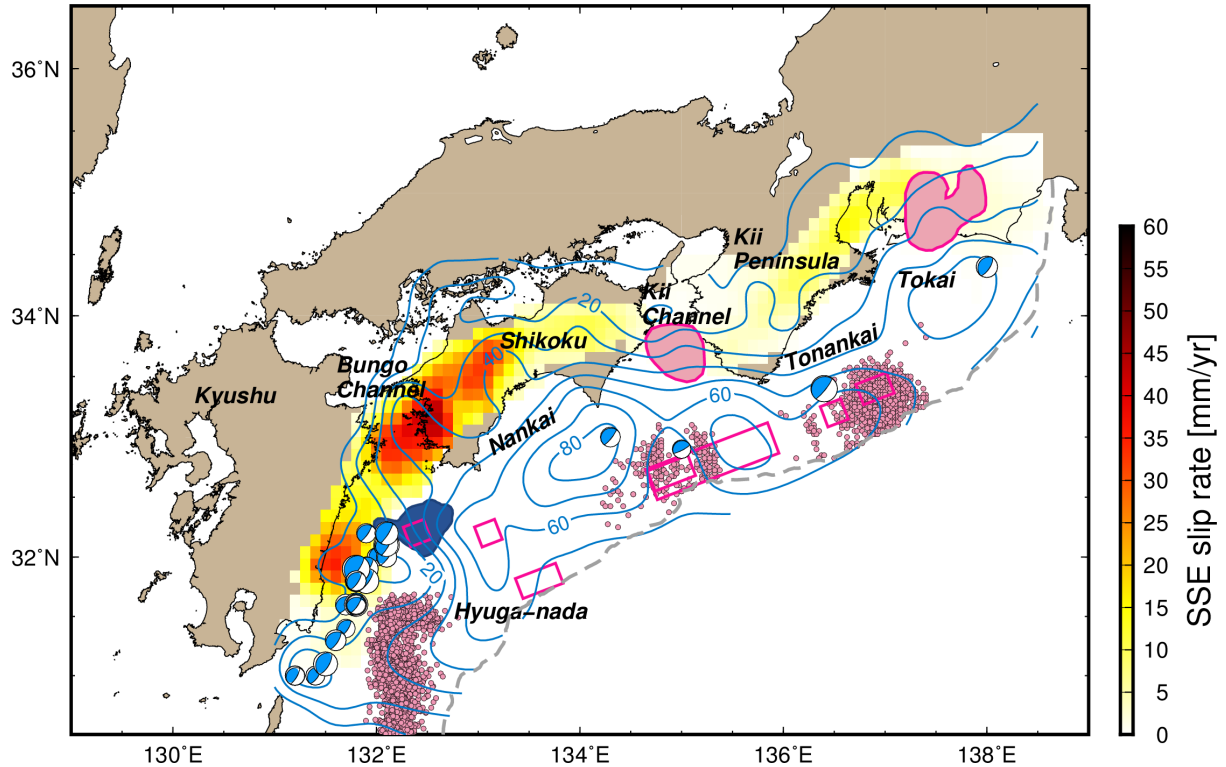


790

791 Figure 7. CMT results for the Hyuga-nada region. Coloured focal mechanisms are our CMT
 792 solutions. The right-hand panels show cross-sections along profiles A-A', B-B' and C-C'.

793 The bathymetry of ETOPO1 (Amante & Eakins 2009), the upper surface, and oceanic
794 Moho of the Philippine Sea Plate (Koketsu *et al.* 2012) along each profile are plotted in
795 the right-hand panels.

796

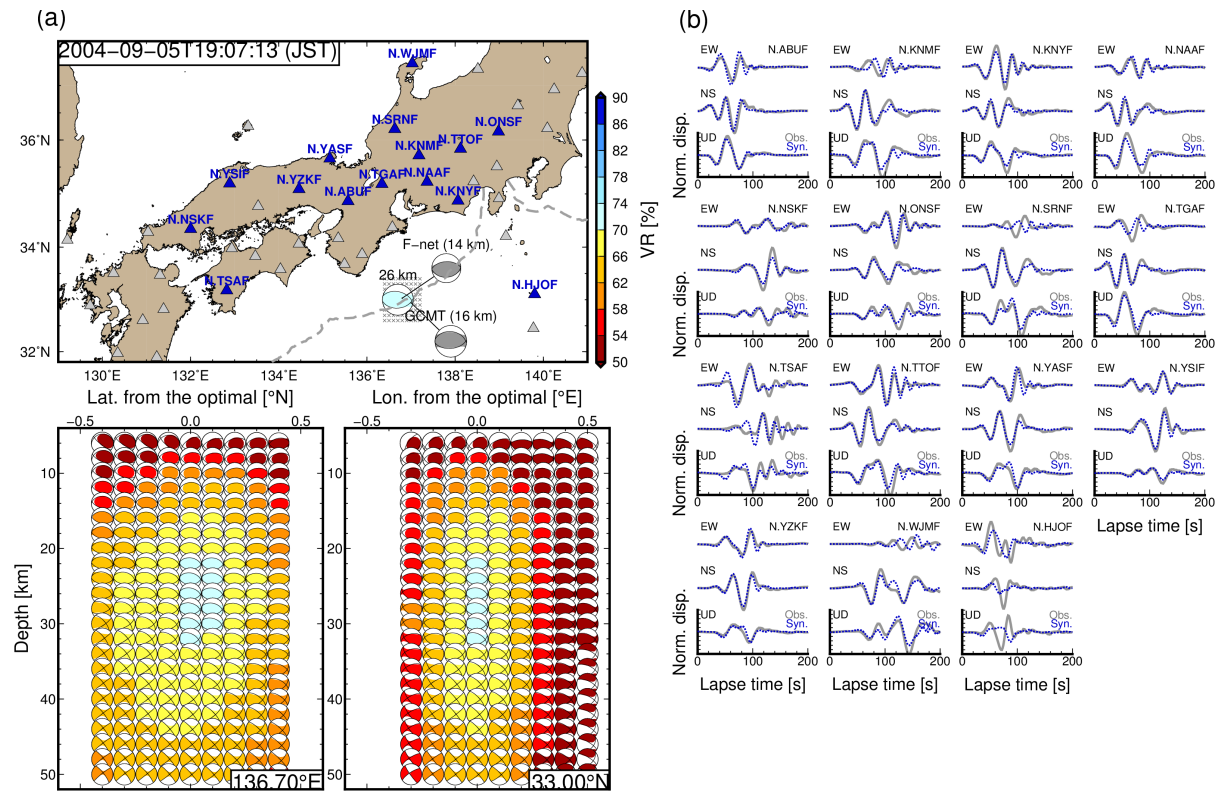


797

798 Figure 8. Spatial distribution of slip behaviours on the plate boundary along the Nankai
799 Trough. Plotted focal mechanisms are low-angle thrust faulting solutions at depths
800 around the plate boundary. The coseismic slip area of the 1968 *Mw* 7.5 Hyuga-nada
801 earthquake (Yagi *et al.* 1998) is shaded in dark blue. SSE slip rates were evaluated from
802 the combined SSE catalogues (Nishimura *et al.* 2013, Takagi *et al.* 2016, 2019). The pink
803 circles indicate the epicentres of the shallow LFTs of the Hyuga-nada and the shallow
804 VLFES in the Tonankai region referred from Yamashita *et al.* (2015) and Takemura,
805 Noda, *et al.* (2019). The pink shaded and enclosed areas indicate the large slip areas of
806 long-term SSEs (Miyazaki *et al.* 2006, Kobayashi 2014) and shallow SSEs (Yokota &
807 Ishikawa 2019), respectively. The blue contour lines indicate the slip-deficit rates
808 [mm/yr] on the plate boundary by Noda *et al.* (2018)

809

810



811

812

Figure 9. CMT results for the M_w 7.2 southeast off the Kii Peninsula earthquake that

813

occurred on 5 September 2004. Grey focal mechanisms are the solutions of the F-net MT

814

and GCMT catalogues. (a) Locations of the optimal solutions, used stations, and depth

815

variations of optimal solutions at each source grid. Colours of the focal mechanisms

816

reflect values of variance reduction between observed and synthetic displacements for

817

25–100 s periods. The numbers above the optimal solutions in (a) are the optimal

818

centroid depths. The grey focal mechanism in (a) is the F-net MT solution of this

819

earthquake; (b) Comparisons of observed and synthetic displacements for 25–100 s

820

periods. Grey solid and blue dotted lines are the observed and synthetic seismograms,

821

respectively. Synthetic seismograms were evaluated by assuming the optimal solution.

822

Amplitudes of both observed and synthetic seismograms at each station were normalised

823

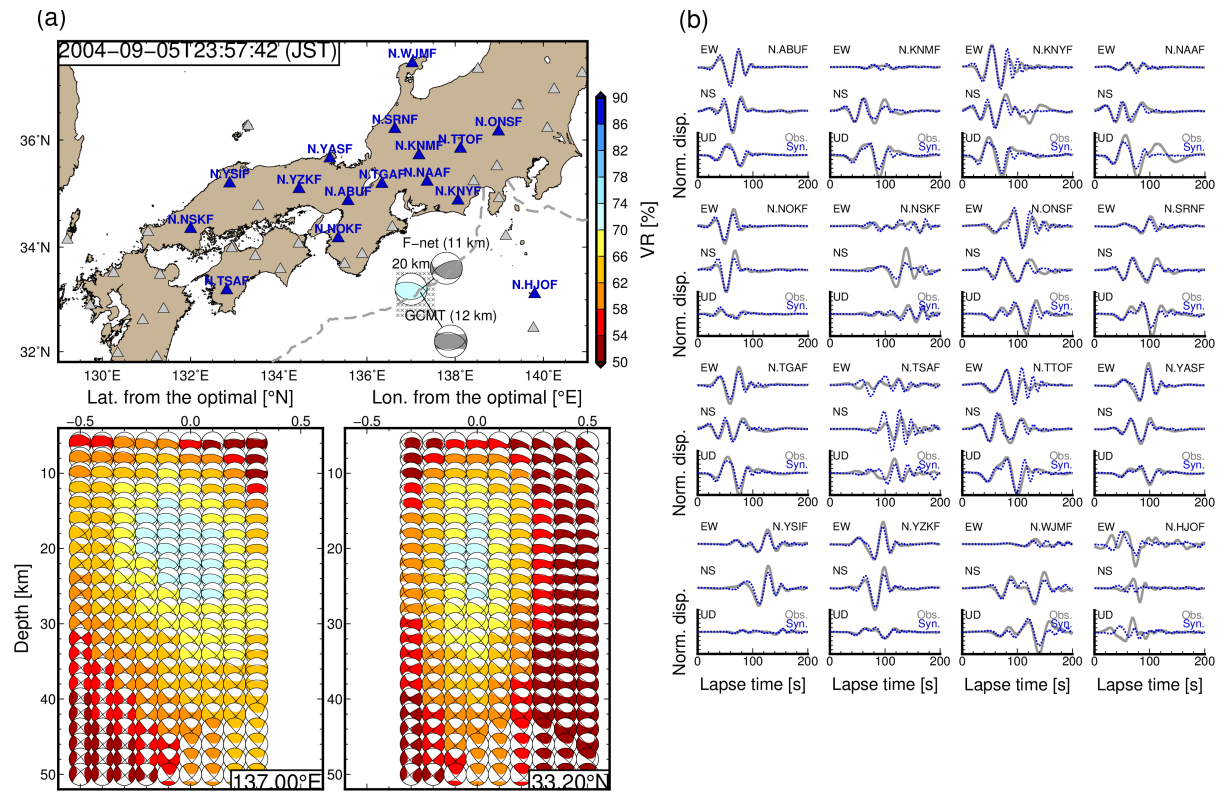
by the maximum amplitude of the observed and synthetic filtered displacements.

824

Detailed source parameters are listed in Table S2.

825

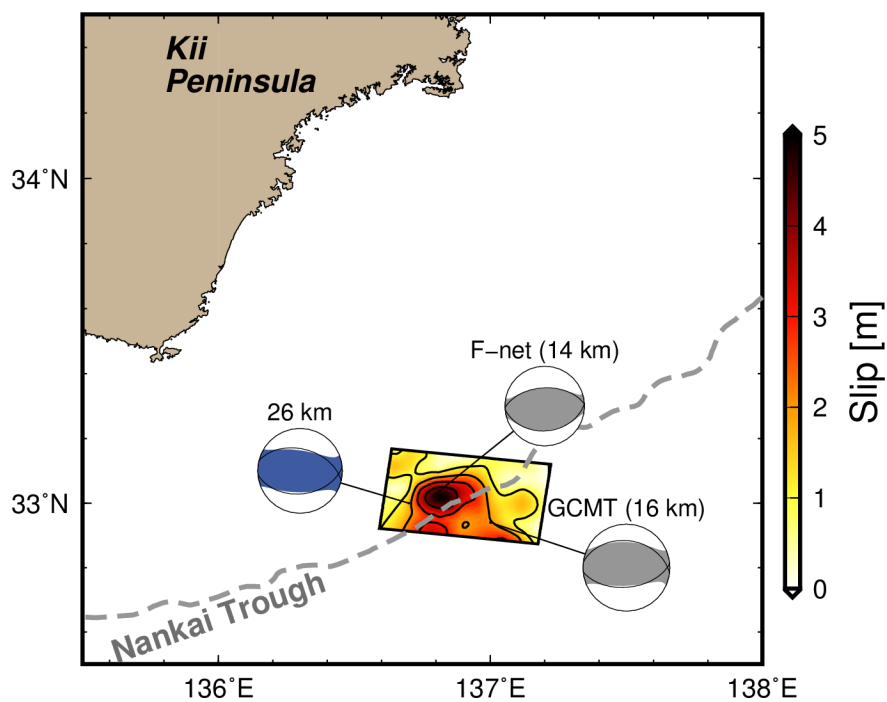
826



827

828 Figure 10. CMT results for the M_w 7.5 southeast off the Kii Peninsula earthquake that
 829 occurred on 5 September 2004. (a) Locations of the optimal solutions, used stations, and
 830 depth variations of optimal solutions at each source grid. Colours of the focal
 831 mechanisms reflect values of variance reduction between observed and synthetic
 832 displacements for 25–100 s periods. The numbers above the optimal solutions in (a) are
 833 the optimal centroid depths. The grey focal mechanism in (a) is the F-net MT solution of
 834 this earthquake; (b) Comparisons of observed and synthetic displacements for 25–100 s
 835 periods. Grey solid and blue dotted lines are the observed and synthetic seismograms,
 836 respectively. Synthetic seismograms were evaluated by assuming the optimal solution.
 837 Amplitudes of both observed and synthetic seismograms at each station were normalised
 838 by the maximum amplitude of the observed and synthetic filtered displacements.
 839 Detailed source parameters are listed in Table S2.

840



841

842 Figure 11. Comparison of the CMT results for the M_w 7.2 southeast off the Kii Peninsula
843 earthquake and other CMT catalogues (Fukuyama *et al.* 1998, Kubo *et al.* 2002, Ekström
844 *et al.* 2012) and finite fault modelling (Okuwaki & Yagi 2018) solutions.

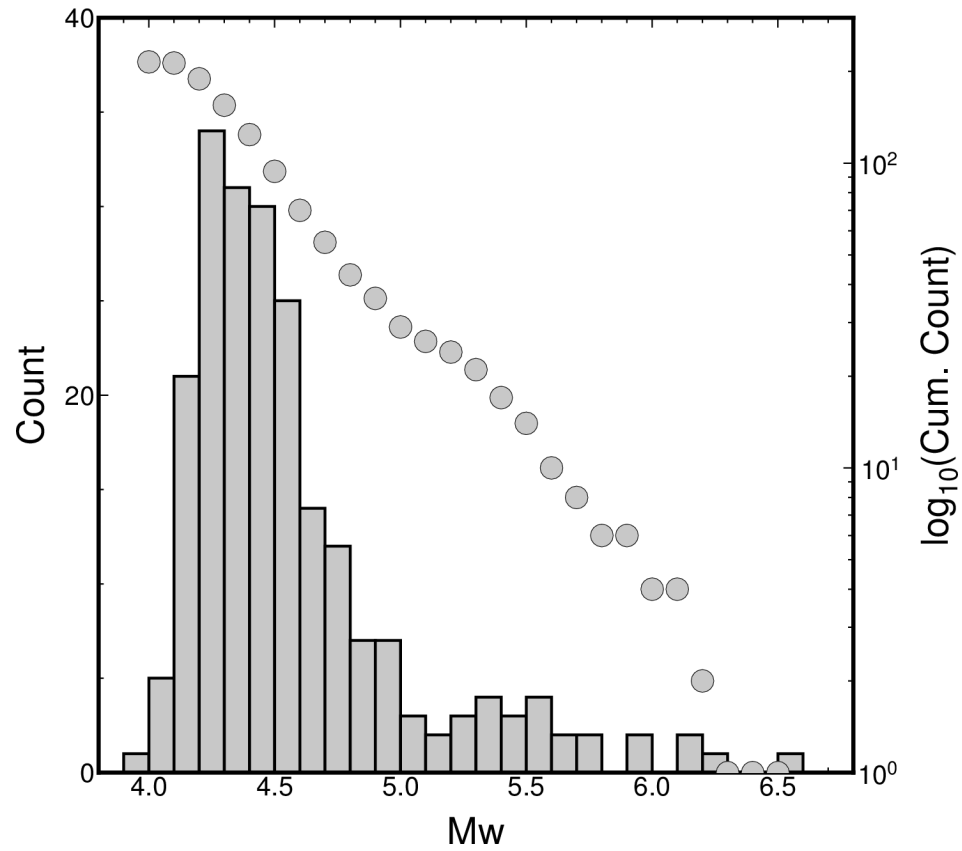


Figure S1. Size distribution of our 3D CMT catalogue.

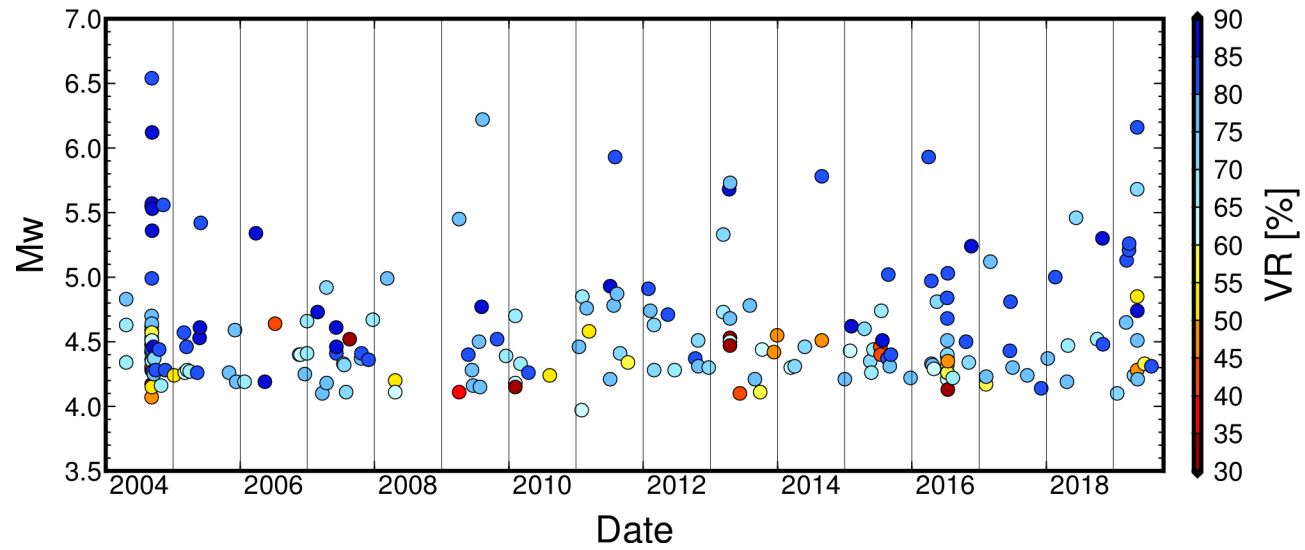


Figure S2. Magnitude-time diagram of our 3D CMT catalogue.

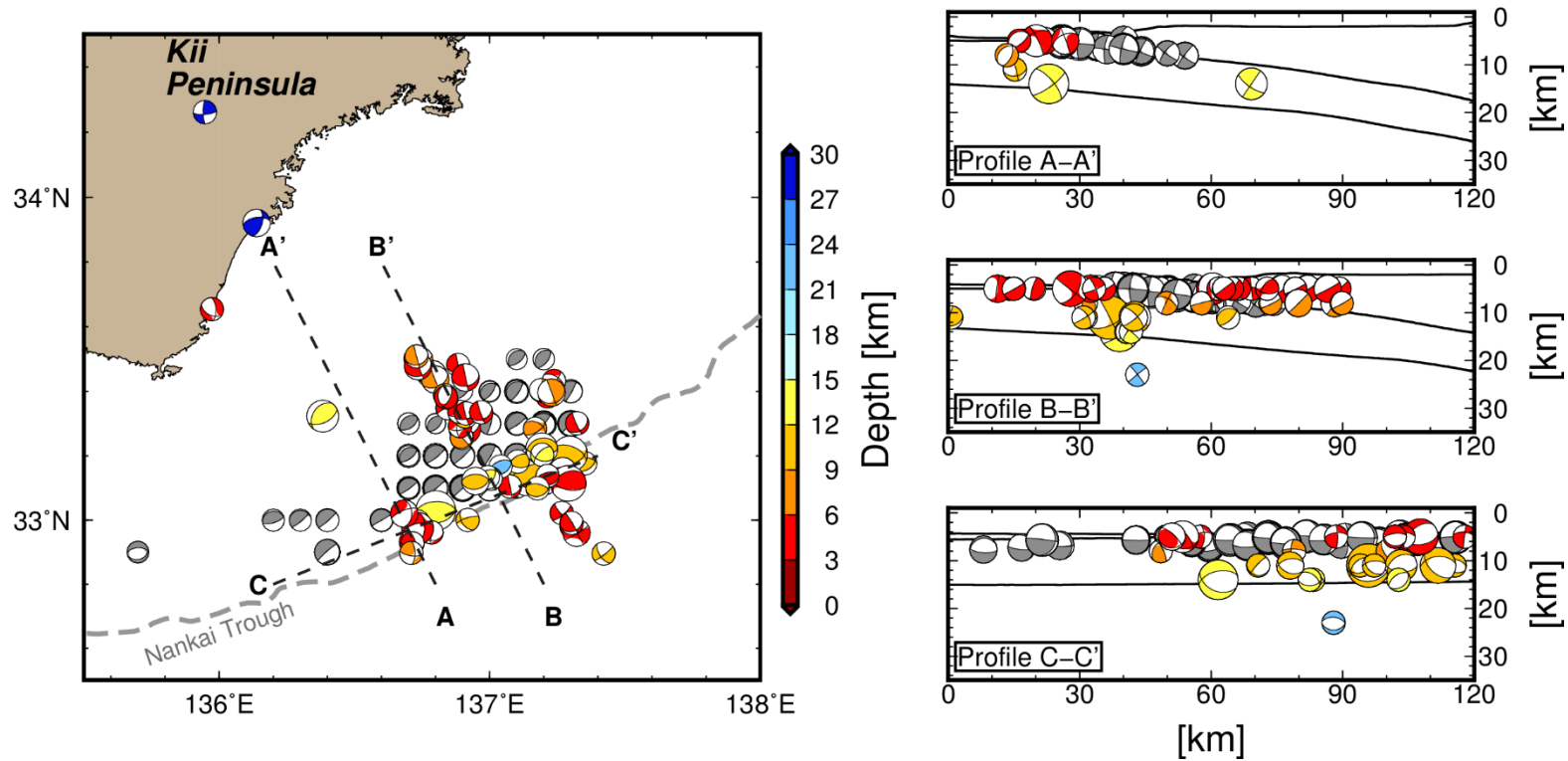


Figure S3. Spatial distribution of CMT solutions southeast of the Kii Peninsula. Coloured focal mechanisms are referenced from the F-net MT catalogue. Grey focal mechanisms are the CMT solutions of shallow VLFs (Takemura, Matsuzawa et al., 2019). Right-hand panels show cross-sections along profiles of A, B and C. The bathymetry of ETOPO1 (Amante & Eakins, 2009), the upper surface, and the oceanic Moho of the Philippine Sea Plate (Koketsu et al., 2012) along each profile are plotted in the right-hand panels.

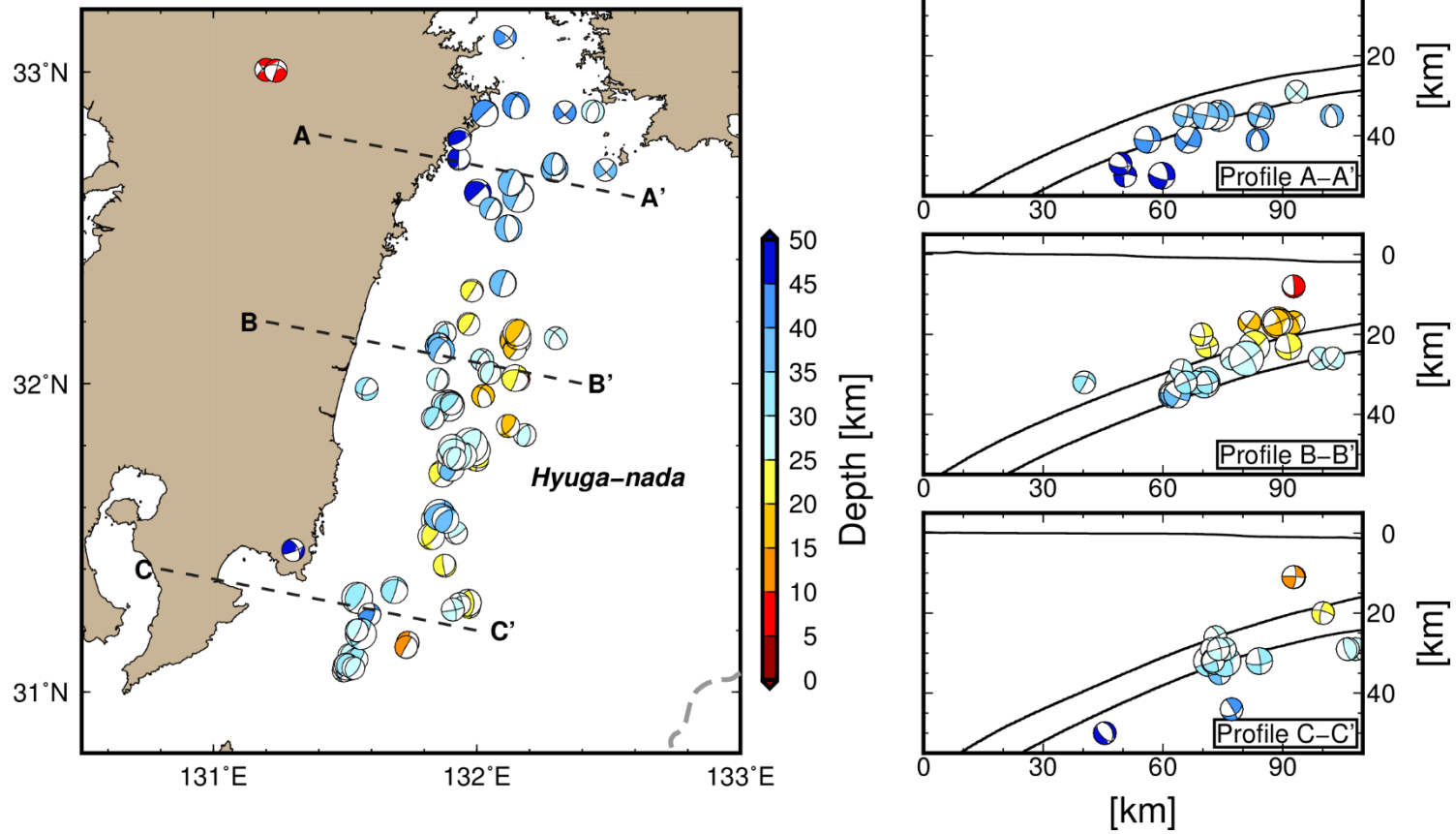


Figure S4. CMT results for the Hyuga-nada region.

Table S1. CMT solutions for all analysed moderate earthquakes.

Centroid time (JST)	Lon.	Lat.	Depth [km]	M_{rr}	$M_{\theta\theta}$	$M_{\phi\phi}$	$M_{r\theta}$	$M_{r\phi}$	$M_{\theta\phi}$	Exp.	Mw	VR [%]
2004-04-20T22:26:31	132.3	33.5	38	-1.357	-1.6975	3.0545	-2.4812	-1.2316	1.3686	22	4.34	67.5
2004-04-21T12:10:42	131.8	31.6	20	0.6864	-0.0375	-0.6489	0.5203	0.6678	-0.2541	23	4.63	68.2
2004-04-21T12:20:53	131.8	31.5	24	1.4508	0.101	-1.5519	0.7083	1.1275	-0.88	23	4.83	78.5
2004-09-06T05:31:03	136.8	33.4	12	0.1901	-1.3058	1.1157	0.5788	0.5214	2.1794	24	5.55	82.9
2004-09-06T07:48:43	137.1	33.1	20	8.4568	-8.4845	0.0277	-0.1917	-2.1778	-2.2808	22	4.57	35.9
2004-09-06T08:59:38	136.9	33.5	14	0.0678	-0.5335	0.4657	0.0528	0.2794	0.9021	23	4.62	72
2004-09-06T11:06:49	137.1	33.6	8	0.3185	1.9433	-2.2618	2.1684	1.7754	-0.2504	22	4.3	65.6
2004-09-06T11:45:40	137.2	33	10	0.2274	-1.8402	1.6128	-1.0266	-0.1838	1.0249	22	4.17	34.7
2004-09-06T13:49:06	136.8	33.4	14	-0.1743	-0.7335	0.9078	-0.4744	0.9627	0.8908	22	4.07	46.5
2004-09-06T13:59:29	136.8	33.5	12	0.0023	-3.4627	3.4604	-0.5306	1.2586	3.9296	22	4.42	77.3
2004-09-06T14:28:53	136.8	33.5	14	0.3208	-2.9967	2.6759	-1.0328	1.7334	2.6699	22	4.36	61.5
2004-09-06T15:35:46	137	33.1	8	0.4137	-2.4345	2.0208	-0.3197	3.3327	3.4922	22	4.42	66
2004-09-06T15:46:49	136.8	33.5	14	0.2543	-4.7452	4.4909	-1.6442	3.1665	4.4559	22	4.51	74.4
2004-09-06T15:54:36	136.7	33.5	16	0.0747	-7.0077	6.933	-1.2333	2.2972	6.3312	22	4.59	80.5
2004-09-06T16:10:06	136.8	33.4	14	0.0901	-3.5793	3.4892	-2.0548	3.9333	3.2224	22	4.48	77.4
2004-09-06T17:20:33	137.3	33.2	24	5.9227	-6.1459	0.2233	-1.5096	0.6317	-1.4292	22	4.47	76.1
2004-09-06T18:11:58	136.9	33	16	0.8177	-1.054	0.2362	-0.7249	-0.0274	0.754	23	4.7	78.6
2004-09-06T19:29:19	137.1	33.2	24	6.406	-8.5764	2.1704	1.9059	-0.0017	-0.7362	22	4.53	68.2
2004-09-06T19:39:48	137.2	33.1	12	1.8829	-5.3833	3.5004	-0.1144	3.0965	0.3394	22	4.44	81.5
2004-09-06T19:59:33	136.6	32.9	8	0.4562	-1.5261	1.07	1.2246	-0.9694	2.5349	22	4.28	59.1
2004-09-07T01:45:30	136.7	33.5	14	-0.0595	-0.7935	0.8531	-0.1833	0.3445	0.6876	23	4.64	78.2

2004-09-07T02:23:38	136.7	32.9	6	0.2361	-0.1379	-0.0982	4.0372	7.3778	3.1622	22	4.57	57
2004-09-07T05:02:49	136.7	33.5	16	-0.0954	-0.7284	0.8238	-0.2423	0.194	1.227	22	4.05	59.4
2004-09-07T08:29:42	137.3	33.2	24	6.76	-8.7612	2.0012	-1.4126	1.3995	-0.0672	25	6.54	81.4
2004-09-07T15:10:05	137.2	33.2	16	3.072	-2.8076	-0.2643	-2.2188	-0.1924	-0.9517	23	4.99	82.9
2004-09-07T15:17:51	137.1	33.7	10	0.3662	1.3792	-1.7454	0.9704	0.8069	0.5912	22	4.15	51.8
2004-09-07T19:58:54	137.2	33.3	10	-0.0713	-3.9503	4.0216	-0.3628	4.9111	3.4998	22	4.51	63.1
2004-09-07T20:56:31	137	33.4	12	-1.194	-1.0187	2.2127	-1.0691	-2.4823	1.6183	22	4.31	42.5
2004-09-08T02:20:25	136.9	32.7	6	0.1269	-2.5415	2.4145	-1.2574	-2.5651	1.8652	22	4.35	67.8
2004-09-08T03:36:24	137.1	33.3	22	2.6349	-2.7037	0.0688	0.8996	-0.2034	-0.1734	24	5.57	85.1
2004-09-08T06:02:15	137.1	33.6	8	0.5073	0.5042	-1.0115	1.6876	0.7738	0.0002	22	4.14	57.6
2004-09-08T23:40:11	137.2	33	8	0.2604	-1.2801	1.0197	-0.4993	0.2195	0.5308	24	5.36	85.9
2004-09-08T23:58:28	137.2	33.2	12	1.4523	-2.0393	0.587	-0.3272	-0.3446	-0.2475	25	6.12	89.3
2004-09-10T11:05:58	136.6	33	10	0.0174	-0.49	0.4726	0.4933	0.9044	2.1698	24	5.53	86.9
2004-09-11T18:05:59	136.7	32.9	10	0.0774	-1.539	1.4616	-0.5858	2.0363	1.9158	22	4.27	83.4
2004-09-17T03:56:29	136.6	32.9	10	-0.6156	-0.5277	1.1433	2.849	3.2868	4.2744	22	4.46	87
2004-09-18T09:48:39	136.8	33.5	12	-0.3511	-1.1663	1.5174	0.16	0.4742	2.562	22	4.25	77.3
2004-09-20T05:17:52	137.2	33.6	8	0.7036	3.2305	-3.9341	2.1988	-0.4975	-1.371	22	4.37	74.1
2004-09-28T00:37:44	137.3	33	10	0.572	-1.861	1.289	-2.1759	1.1947	1.3091	22	4.28	83
2004-10-03T08:00:21	136.8	33.4	12	-1.4439	-0.6286	2.0725	0.4632	0.2373	0.1244	22	4.12	71.9
2004-10-17T07:05:42	137.2	33.2	22	3.9515	-5.1385	1.187	-1.2903	-2.6526	-1.8995	22	4.44	82
2004-10-27T21:27:31	135.2	33.6	34	-0.4372	-1.7282	2.1655	0.0469	-0.4457	-0.8677	22	4.16	69.7
2004-11-09T00:07:28	138.4	33.8	16	2.1695	-2.6496	0.4801	-1.013	0.6477	0.3658	24	5.56	82.9
2004-11-19T05:46:28	137.1	33.2	12	2.9056	-3.3445	0.4389	-0.7283	-0.4218	-0.4779	22	4.28	80.9
2005-01-05T23:49:13	139.3	34.2	8	1.2691	-3.1909	1.9218	0.0929	0.5325	0.6501	22	4.24	53.4

2005-03-01T06:59:46	136.9	33.4	12	1.001	-5.8171	4.8162	3.1308	1.8919	6.0684	22	4.57	84.1
2005-03-05T14:58:50	131.2	31.4	42	0.8974	-2.0131	1.1156	0.8395	1.2316	2.0335	22	4.26	65
2005-03-14T19:49:32	137	33.1	28	5.7175	-4.7523	-0.9652	-2.4026	-0.055	-2.0364	22	4.46	82.3
2005-03-19T11:34:10	137.2	33	24	2.9604	-3.5697	0.6093	-0.3674	0.0348	-0.3644	22	4.28	64.7
2005-04-01T09:41:49	131.4	31	32	2.3644	-0.8107	-1.5537	1.1653	1.8244	-1.0436	22	4.27	68.1
2005-05-12T04:22:51	132	32.1	28	-1.6099	-1.0197	2.6296	1.3696	1.5371	0.5932	22	4.26	82.7
2005-05-25T20:31:30	132.3	33.4	46	-3.1031	-4.2984	7.4014	3.3402	2.2254	-1.7336	22	4.53	85.3
2005-05-27T03:17:19	133.7	34	36	-0.4494	-0.5497	0.9991	-0.4676	-0.3466	0.0844	23	4.61	89.6
2005-05-31T11:04:15	131.5	31.3	30	0.9813	0.0704	-1.0517	0.9508	0.8888	-0.3208	24	5.42	81
2005-11-01T12:47:35	135.1	33.8	46	-1.0601	0.5529	0.5072	-2.2706	-1.4095	1.1458	22	4.26	78.4
2005-12-03T10:39:02	137	33.1	26	10.1208	-7.3714	-2.7493	0.143	0.8015	-3.3126	22	4.59	77.6
2005-12-03T11:01:22	137	33.1	28	6.9856	-4.731	-2.2546	1.1887	1.4634	-4.1805	22	4.52	73.3
2005-12-10T18:32:09	132	32	26	1.4435	-0.1028	-1.3406	1.2512	1.4464	-0.4202	22	4.19	76.2
2006-01-24T21:36:47	131.7	31.4	20	1.4303	-0.585	-0.8453	1.0039	1.6058	-0.7574	22	4.19	67.2
2006-03-27T11:50:26	132.2	32.6	34	-0.0067	-0.2097	0.2164	0.662	1.1059	-0.028	24	5.34	86.6
2006-05-15T01:42:11	135.2	34.2	6	1.4901	1.0789	-2.569	-0.0809	0.6344	-0.7802	22	4.19	86.2
2006-07-09T17:48:06	139.4	34.3	14	0.2085	-0.7853	0.5769	-0.0862	0.1949	-0.8847	23	4.64	40.9
2006-11-18T01:08:36	132	31.9	32	-2.5129	-2.3879	4.9008	2.409	-0.5069	-1.1892	22	4.4	75.1
2006-11-25T15:39:45	132.1	32	10	2.5354	-0.9052	-1.6302	2.6184	3.5397	-0.3243	22	4.4	60.1
2006-12-19T03:28:50	131.6	32	42	-1.3385	1.3769	-0.0384	-0.1348	1.8295	1.909	22	4.25	79.2
2006-12-31T02:49:32	139.4	34.2	12	-0.4855	-0.0157	0.5012	-0.615	0.1021	-0.9646	23	4.66	67.2
2006-12-31T03:42:11	139.3	34.2	12	-3.5025	2.406	1.0965	1.3953	-0.4392	-3.8411	22	4.41	69
2007-02-25T20:41:22	136.9	33.1	22	1.4403	-1.4342	-0.0061	0.6018	-0.234	-0.1851	23	4.73	85.6
2007-03-23T16:20:53	136.9	33.4	10	0.0059	-0.9814	0.9755	0.2088	0.6617	1.3486	22	4.1	76.6

2007-04-15T12:19:29	136.4	34.8	14	2.738	-0.2696	-2.4684	0.5046	0.7611	1.2386	23	4.92	71.7
2007-04-15T18:34:45	136.4	34.8	12	1.9049	0.3127	-2.2177	0.8835	-0.5492	0.1329	22	4.18	77.1
2007-04-26T09:02:55	133.6	33.9	34	0.4223	-3.5005	3.0782	-0.3535	0.9473	0.6558	23	4.96	88.6
2007-06-06T23:42:49	131.5	33.3	10	-0.2061	0.9777	-0.7716	0.0837	0.3929	-0.2776	23	4.61	87.3
2007-06-07T17:22:15	131.5	33.3	8	-1.5836	5.0032	-3.4196	0.3935	2.2127	-1.7062	22	4.41	84.5
2007-06-07T20:50:39	131.5	33.3	8	-2.1527	5.917	-3.7642	-0.8056	2.8071	-1.6272	22	4.46	85.8
2007-07-16T17:24:18	135.9	34.3	38	-0.1656	0.321	-0.1555	0.1414	-0.7578	-3.897	22	4.33	61.3
2007-07-20T17:15:25	139.4	34.8	12	1.0774	0.0622	-1.1396	-1.0415	-1.0824	-3.2583	22	4.32	71.5
2007-07-31T10:22:40	131.9	32.2	26	1.4741	0.1401	-1.6142	-0.2327	0.8087	-0.4541	22	4.11	70.2
2007-08-19T10:21:55	138.6	34	50	-0.8675	2.5606	-1.6931	3.3543	-6.004	-2.0221	22	4.52	31.5
2007-10-21T02:09:27	131.9	32.2	28	2.0351	-1.1698	-0.8653	2.1099	3.2966	-1.3251	22	4.37	76.8
2007-10-22T09:36:00	139.1	34.2	14	2.3922	-4.9035	2.5113	-1.501	2.5717	0.6986	22	4.41	83
2007-11-29T20:17:48	131.9	32.7	44	-0.1989	-1.1422	1.3411	0.5946	4.0001	1.1751	22	4.36	83.3
2007-12-23T02:49:06	131.6	31.2	26	0.3196	-0.4838	0.1642	0.231	1.001	-0.6548	23	4.67	69.4
2008-03-10T10:44:31	131.8	31.8	18	2.1467	-0.885	-1.2617	1.7677	2.7101	-0.8194	23	4.99	75.5
2008-04-22T18:07:20	131.4	31	28	0.8657	-0.9318	0.0661	-1.2227	-1.0644	-1.7256	22	4.2	54.3
2008-04-22T18:26:11	131.5	31	24	0.5488	-0.919	0.3702	-1.0332	-0.8558	-0.9915	22	4.11	62.9
2009-04-05T18:36:28	131.9	31.9	26	1.0367	-0.2014	-0.8353	0.9717	1.2803	-0.3601	24	5.45	78.2
2009-04-05T18:53:18	131.8	31.9	28	0.613	-0.416	-0.197	0.9975	1.3747	0.4606	22	4.11	37.3
2009-05-25T20:26:21	137.8	34.7	28	0.3139	-4.7617	4.4478	-0.1079	1.6215	0.7652	22	4.4	82.6
2009-06-14T19:17:54	132.1	33.1	50	0.1692	-2.7974	2.6282	-0.3131	1.8257	0.0194	22	4.28	78.2
2009-06-20T04:22:18	135	32.9	6	0.8329	-0.6077	-0.2252	1.8332	0.9457	-0.3284	22	4.16	76.6
2009-07-22T23:51:01	134.3	33	16	2.5675	-1.5958	-0.9717	3.9223	5.157	-1.5788	22	4.5	77.4
2009-07-28T05:30:55	131.8	32	32	-1.0858	-0.0334	1.1193	0.8299	1.4609	0.5419	22	4.15	77.5

2009-08-05T12:51:14	132.1	32.6	34	-1.2827	-0.1958	1.4785	0.0996	1.1442	0.0227	23	4.77	85
2009-08-11T05:07:09	138.4	34.8	22	2.0222	-2.2667	0.2445	1.0673	0.7672	0.9577	25	6.22	79.5
2009-10-29T02:37:09	132	32.4	32	-4.0859	-0.0828	4.1687	2.26	5.8198	0.9274	22	4.52	81
2009-12-16T14:12:51	133.4	33.2	30	0.3214	-4.1432	3.8218	-2.6779	-0.1908	-0.0985	22	4.39	69.8
2010-02-04T17:41:59	131.5	31.5	10	-1.2762	0.6802	0.596	-0.9353	-1.8535	0.0247	22	4.18	61.7
2010-02-04T20:30:09	131.5	31.5	8	-0.3484	0.2543	0.0942	-0.5176	-1.2826	0.0114	23	4.7	65.3
2010-02-04T20:35:22	131.5	31.1	28	0.1496	0.5215	-0.6711	-0.5513	-1.7085	-0.907	22	4.15	33.1
2010-03-05T06:49:56	139.5	33.8	16	-0.5247	-2.8574	3.3822	0.6979	-0.0789	-2.2332	22	4.33	69.1
2010-04-17T05:34:56	132.5	33.6	40	-2.5829	0.5543	2.0287	1.3273	-0.9056	-1.1129	22	4.26	84.9
2010-08-10T21:24:07	132.4	32.9	32	-2.7518	0.121	2.6308	0.4307	-0.2828	0.8577	22	4.24	51.6
2011-01-16T20:33:23	133.8	34	36	-0.1685	-3.5513	3.7198	-0.694	0.9807	4.8382	22	4.46	78.9
2011-02-01T02:32:25	132	31.7	22	0.8643	-0.3696	-0.4947	0.2119	0.5494	-0.5995	22	3.97	62.9
2011-02-04T18:11:24	131.5	31	32	2.1193	-0.4547	-1.6646	0.9618	0.8368	-0.6417	23	4.85	68.8
2011-02-28T09:04:34	131.8	32.1	34	-1.1333	-0.2285	1.3618	0.7021	0.9012	0.3583	23	4.76	78.5
2011-03-12T22:11:02	136.8	33	10	-1.3814	-2.7719	4.1533	3.2202	1.0853	8.0288	22	4.58	52.3
2011-07-05T19:18:42	135.2	34	8	2.6477	-0.4269	-2.2208	-0.075	1.2127	-1.4264	23	4.93	86.5
2011-07-05T19:34:54	135.2	34	8	2.2075	-0.3256	-1.8819	0.1836	1.097	-1.152	22	4.21	75.3
2011-07-24T23:32:12	136.1	34	38	1.0659	-0.8068	-0.2591	-0.4365	0.8299	-1.316	23	4.78	78.5
2011-08-01T23:58:13	138.5	34.7	18	8.7245	-8.3238	-0.4008	4.6443	0.4007	0.2345	24	5.93	81.6
2011-08-12T04:37:46	138	34.4	10	1.7337	-0.545	-1.1887	1.0074	1.5403	-0.7179	23	4.87	76.4
2011-08-28T09:52:03	131.2	31	30	3.6473	-2.181	-1.4662	1.7998	3.4005	-1.3799	22	4.41	71
2011-10-10T19:19:28	134.1	34	38	-2.0054	-1.171	3.1764	-2.5103	1.3851	-0.4369	22	4.34	55.4
2012-01-30T03:18:21	132	32.6	44	0.177	-0.8981	0.7212	2.0799	1.8079	-0.2874	23	4.91	84.5
2012-02-09T12:55:15	131.6	31.3	24	1.0229	-0.6082	-0.4147	0.5156	1.1158	-0.6235	23	4.74	77.6

2012-02-29T01:23:02	131.9	31.8	18	0.6718	-0.1089	-0.5629	0.5605	0.6858	-0.202	23	4.63	70.7
2012-02-29T19:33:33	131.8	31.6	18	1.0949	0.179	-1.2738	1.1601	2.8352	0.0018	22	4.28	73
2012-05-14T12:36:44	131.7	31.6	24	0.8837	-0.634	-0.2497	0.5745	0.9543	-0.5517	23	4.71	82.8
2012-06-20T03:35:33	132.3	32.1	30	-1.8684	-1.2806	3.149	1.7229	-0.7716	-0.2973	22	4.28	68.9
2012-10-10T05:49:34	132.5	32.7	26	0.0137	-4.3042	4.2905	-0.5896	0.4697	0.8573	22	4.37	80.9
2012-10-26T01:54:14	131.9	31.9	28	5.5318	-1.8796	-3.6522	3.7555	2.9964	-2.4523	22	4.51	74.9
2012-10-27T04:44:36	133.5	33.5	32	0.0585	-3.1104	3.052	2.0373	-0.4653	-0.1491	22	4.31	78.8
2012-12-22T15:15:29	132.3	33.6	44	-3.1873	0.2798	2.9075	0.0741	1.6438	-0.4459	22	4.3	74.7
2013-03-11T18:34:52	131.8	31.6	22	0.7453	-0.0027	-0.7427	0.5966	0.7457	-0.2558	24	5.33	74.6
2013-03-11T18:59:45	131.8	31.6	18	1.0296	-0.1435	-0.886	0.8015	0.9362	-0.2943	23	4.73	68.1
2013-04-13T05:33:18	134.8	34.4	14	3.5282	0.2016	-3.7298	0.1173	-1.9891	0.7873	24	5.68	86.6
2013-04-17T10:15:23	139.4	34.1	12	4.0018	1.2519	-5.2536	-3.6206	0.7026	-4.971	22	4.53	26.4
2013-04-17T11:13:58	139.5	34	6	0.6066	2.9894	-3.596	1.2982	-0.0078	-6.0277	22	4.5	62.6
2013-04-17T11:16:19	139.4	34.1	10	-1.5059	3.8416	-2.3357	-1.1352	-1.6548	-4.9695	22	4.47	32
2013-04-17T12:22:13	139.4	34.1	10	-0.0744	0.7911	-0.7167	-0.364	-0.2789	-0.9958	23	4.68	75.5
2013-04-17T17:57:37	139.4	34	8	0.2804	-1.7017	1.4213	-0.2263	-2.0019	-4.3235	24	5.73	78.3
2013-06-10T10:11:02	139.4	33.2	10	0.7045	-0.6324	-0.0721	-1.5068	0.7294	0.1011	22	4.1	41.5
2013-08-03T09:56:14	137.5	34.6	32	-1.8414	0.5047	1.3367	-0.2712	-0.2477	0.7867	23	4.78	78.6
2013-08-18T08:01:00	139.4	33.3	14	-0.2568	-0.014	0.2707	-0.1908	0.3922	-1.2715	23	4.69	67.5
2013-08-30T17:32:25	135.9	33.7	8	-1.7882	0.0163	1.7719	-0.1965	-0.5021	-1.8316	22	4.21	76.1
2013-09-28T04:37:48	131.5	31.2	28	1.4157	-1.101	-0.3147	0.1475	1.052	-0.7716	22	4.11	58.2
2013-10-08T20:45:22	131.9	31.8	20	3.3567	-0.682	-2.6747	3.0437	3.6202	-1.457	22	4.44	62.6
2013-12-12T11:25:14	131.2	31.2	30	-2.6186	0.3605	2.258	-2.6677	-3.857	-0.0001	22	4.42	48.1
2013-12-29T10:17:50	139.5	33.3	50	-2.3213	-0.2305	2.5518	-3.373	1.671	-6.9566	22	4.55	48.6

2014-03-13T07:35:54	131.4	31	26	3.1932	-0.7432	-2.4501	1.0824	0.8837	-1.5896	22	4.3	63.2
2014-04-04T00:46:43	132.1	32.5	34	-1.606	-0.0928	1.6988	1.7584	2.7185	0.7315	22	4.31	74.4
2014-05-29T09:18:00	139.4	33.3	14	-5.8398	2.8701	2.9697	1.5234	-0.5435	-3.0242	22	4.46	73
2014-08-29T04:14:36	132.1	32.1	22	2.385	-1.3919	-0.9931	2.3946	4.4971	-1.8215	24	5.78	82.6
2014-08-29T04:32:04	132.1	32.1	22	2.5535	-1.0894	-1.4641	4.1729	5.2609	-1.6985	22	4.51	45
2015-01-02T01:14:07	131.9	32.1	32	-0.5414	-0.1113	0.6528	0.444	2.4635	0.1783	22	4.21	79.5
2015-01-30T16:45:55	131.8	31.8	18	3.2694	-0.2876	-2.9817	2.9076	3.5835	-0.6984	22	4.43	64
2015-02-06T10:25:11	134.4	33.8	10	0.0838	0.8859	-0.9698	-0.1325	0.2548	-0.4568	23	4.62	86
2015-04-18T18:34:55	132.1	32	16	0.4897	-0.1686	-0.3212	0.5431	0.7164	-0.1401	23	4.6	70.7
2015-05-19T15:13:19	139.4	34.4	14	-0.3559	-0.6007	0.9565	-0.0486	0.0517	-4.184	22	4.35	70.4
2015-05-26T01:35:22	131.9	31.8	22	2.1759	-0.2887	-1.8872	1.5653	1.5741	-0.677	22	4.26	65.8
2015-06-06T16:28:13	139.3	33	10	-1.8498	-0.4521	2.3019	0.7025	2.7706	-4.5809	22	4.44	69
2015-07-13T15:52:35	131.8	31.4	28	-2.7135	-1.3844	4.0979	-0.2721	4.7081	1.8082	22	4.46	42.3
2015-07-15T16:18:47	139.2	33.2	12	0.3285	-2.1215	1.793	-2.7498	3.6604	-0.3661	22	4.4	44.7
2015-07-19T02:13:43	131.3	31.3	20	-1.066	0.2193	0.8467	-0.8225	-0.984	0.13	23	4.74	67.6
2015-07-24T17:53:34	132.4	33.4	40	-5.9261	-0.1244	6.0505	0.3362	4.3824	-0.2904	22	4.51	86.6
2015-08-21T16:54:35	132.2	33.3	44	-3.6329	0.5234	3.1095	1.6506	2.2531	1.1541	22	4.37	81.5
2015-08-26T07:51:36	131.9	32.1	34	-2.0236	-1.1574	3.181	2.4139	1.4665	1.3746	23	5.02	82.7
2015-09-02T16:07:47	134.6	33.3	12	-2.9105	1.6774	1.2331	-0.5466	1.9276	-1.7628	22	4.31	76.7
2015-09-08T20:22:39	138.4	34.7	18	0.894	-0.8622	-0.0318	1.2257	2.2265	4.1443	22	4.4	81.5
2015-12-25T11:20:36	134.5	33.5	32	-0.038	-2.4965	2.5345	-0.6622	0.5152	0.198	22	4.22	77.1
2016-04-01T11:39:09	136.4	33.4	10	3.2075	-1.9851	-1.2225	5.7603	7.4312	-1.554	24	5.93	80.8
2016-04-16T07:11:37	131.4	33.3	6	0.0122	2.6717	-2.6839	1.5596	1.1468	-1.4731	23	4.97	83.4
2016-04-16T14:03:56	131.2	33	6	0.3492	3.3242	-3.6734	0.3092	1.3586	-1.0284	22	4.33	71

2016-04-21T23:20:37	134.3	33.5	30	-0.5746	-3.3915	3.9661	0.4438	0.2301	-0.3544	22	4.32	76.5
2016-04-29T15:09:34	131.4	33.3	6	-0.1864	3.1013	-2.9149	1.0305	0.4916	-1.0067	22	4.29	63.2
2016-05-16T17:50:20	131.8	31.8	18	1.2032	-0.3495	-0.8537	1.0247	1.3676	-0.359	23	4.81	73.7
2016-07-11T15:22:01	139.4	33.3	14	-1.7994	0.5647	1.2346	0.6467	0.9714	-1.1017	23	4.84	80.3
2016-07-11T16:58:34	139.4	33.3	14	-4.0329	1.8471	2.1858	1.9735	1.2067	-1.9929	22	4.38	76.1
2016-07-11T17:33:02	139.5	33.2	10	-3.1075	1.7145	1.393	1.7574	1.019	-1.7902	22	4.32	58.8
2016-07-11T17:39:40	139.4	33.3	14	-1.9739	0.697	1.2769	1.2312	0.6247	-1.4048	22	4.21	61.5
2016-07-11T19:31:11	139.4	33.3	14	-2.7229	0.9532	1.7697	1.0057	0.9592	-1.3753	22	4.26	70.5
2016-07-12T05:54:20	139.5	33.3	14	-1.1808	0.384	0.7968	0.493	-0.1699	-0.6492	23	4.68	80.1
2016-07-12T06:56:52	139.4	33.3	12	-3.8721	0.6637	3.2084	2.2695	-1.0943	-2.4253	22	4.4	73.1
2016-07-12T07:34:02	139.4	33.3	12	-5.631	3.1221	2.5089	2.091	2.5566	-4.3533	22	4.51	75.4
2016-07-13T06:24:52	139.5	33.2	12	-2.541	1.4209	1.1201	1	0.6946	-1.727	22	4.26	57.3
2016-07-14T11:05:56	139.4	33.3	14	-0.9717	0.2777	0.694	0.8119	1.1479	-1.1006	22	4.13	20.4
2016-07-14T11:07:07	139.4	33.3	14	-3.3662	1.3522	2.014	1.5784	1.4813	-2.2552	22	4.35	49.9
2016-07-14T11:17:27	139.4	33.3	12	-3.9403	2.0106	1.9298	1.4	1.1681	-2.2075	23	5.03	80.3
2016-08-10T16:25:57	131.8	31.8	18	1.3331	-0.6217	-0.7114	1.2939	1.9569	-0.4921	22	4.22	69.6
2016-10-22T03:33:45	131.9	32.8	50	3.9676	-4.2294	0.2617	4.7291	3.137	-0.5439	22	4.5	83.1
2016-11-05T16:57:33	131.9	31.8	18	2.5509	-0.7718	-1.7791	1.9785	2.6455	-0.6888	22	4.34	73.6
2016-11-19T11:48:01	135.4	33.9	48	-3.6325	-4.0604	7.6929	2.7175	-0.4451	-5.7836	23	5.24	87.6
2017-02-07T16:21:51	131.5	31.5	18	-0.9278	0.9309	-0.0031	-0.566	-1.9684	0.0394	22	4.17	56.1
2017-02-08T03:19:27	134.6	33.4	32	-0.0637	-2.3988	2.4625	-1.0362	0.3671	-0.7235	22	4.23	77.8
2017-03-02T23:53:43	132.1	32.7	34	-3.5332	-0.7299	4.2631	1.5145	4.2689	0.786	23	5.12	79.7
2017-06-16T22:39:51	131.8	31.9	26	3.381	-0.6083	-2.7727	2.94	3.2205	-1.3037	22	4.43	80.1
2017-06-20T23:27:40	132	32.9	40	-0.4731	-0.1317	0.6049	1.2724	1.3717	0.6915	23	4.81	81.4

2017-07-02T00:58:22	131.3	33	10	-1.3107	2.2919	-0.9813	0.0344	-1.299	2.6235	22	4.3	79.7
2017-09-19T18:33:08	132.3	33.4	40	-2.5607	0.377	2.1837	0.0234	1.3128	-0.8112	22	4.24	78.7
2017-12-04T16:54:12	131.9	32.2	30	0.3743	-1.0503	0.676	0.7958	1.6386	-0.2401	22	4.14	80.7
2018-01-09T05:52:07	132.2	33.8	50	-2.3888	-1.4059	3.7947	0.6465	2.9379	-0.2507	22	4.37	75.8
2018-02-19T03:31:37	132.2	32.9	40	-2.8399	-0.5824	3.4224	1.7575	1.4811	-0.2862	23	5	84.7
2018-04-23T05:49:37	139.2	34.3	10	0.8199	-2.3806	1.5607	0.9054	0.2384	-0.7391	22	4.19	77.3
2018-04-28T13:27:34	131.9	32	6	-2.3439	0.0911	2.2527	-3.7815	-4.529	0.0852	22	4.47	68.7
2018-06-12T04:54:21	131.5	31.1	30	1.4716	-0.4028	-1.0688	0.6843	1.1412	-0.5431	24	5.46	74
2018-10-04T17:20:53	131.2	31	30	5.9256	-3.3772	-2.5483	2.2505	4.7264	-2.2398	22	4.52	68.2
2018-11-02T16:53:54	135.2	33.7	40	-0.4302	0.035	0.3952	0.2262	-0.6334	-0.8114	24	5.3	89.3
2018-11-05T08:19:14	135.3	33.7	46	-0.6427	-4.0587	4.7014	2.194	-1.7504	-4.0383	22	4.48	81.7
2019-01-21T23:17:08	132.4	32.9	28	0.0401	-1.7516	1.7115	-0.2722	0.271	0.3018	22	4.1	74.6
2019-03-11T15:37:49	132.7	33.2	34	-0.3189	-0.8166	1.1355	0.3179	0.2012	-0.5394	23	4.65	79.2
2019-03-13T13:48:47	134.9	33.8	38	0.5685	-5.9744	5.4058	-0.8286	-1.857	-1.6438	23	5.13	84.2
2019-03-27T09:11:23	132.1	32.1	22	3.5887	-1.6418	-1.9469	3.2572	6.4347	-2.7917	23	5.21	83.7
2019-03-27T15:38:04	132.1	32.2	22	3.8583	-1.2031	-2.6552	4.6751	7.613	-2.3919	23	5.26	84.5
2019-04-23T07:49:50	131.2	31.3	24	-1.4358	0.4849	0.9509	-1.2569	-2.2809	-0.0562	22	4.24	73.1
2019-05-10T07:43:24	131.9	31.8	20	2.4441	-0.6387	-1.8054	2.1455	2.7885	-0.7343	24	5.68	73.1
2019-05-10T08:48:46	131.8	31.9	26	1.0889	-0.1965	-0.8924	1.1381	1.5277	-0.4371	25	6.16	80.1
2019-05-10T09:07:37	131.9	31.8	26	2.005	-0.0686	-1.9364	0.9407	0.9768	-0.1032	23	4.85	50.8
2019-05-10T13:53:53	131.9	31.8	22	1.9288	0.4866	-2.4154	2.0226	1.1028	-0.8503	22	4.28	47.8
2019-05-10T20:40:38	131.8	31.8	28	4.575	-2.3805	-2.1945	2.6548	5.059	-2.0404	22	4.51	77.6
2019-05-11T08:59:39	132.3	32.7	32	-0.7341	-0.2024	0.9365	0.3296	1.3177	-0.1167	23	4.74	87.8
2019-05-12T15:07:42	132.3	32.7	32	-1.6641	-0.1141	1.7782	0.2608	1.938	-0.0225	22	4.21	77.1

2019-06-19T11:35:45	131.2	31	32	2.5038	-1.4996	-1.0042	1.1971	2.9308	-0.7981	22	4.33	58.6
2019-07-27T02:11:47	131.8	31.6	24	1.7323	-1.5534	-0.1789	1.4295	2.5845	-1.4655	22	4.31	80
2004-04-20T22:26:31	132.3	33.5	38	-1.357	-1.6975	3.0545	-2.4812	-1.2316	1.3686	22	4.34	67.5

Table S2. CMT solutions for the M_w 7.2 and 7.5 earthquakes.

Centroid time (JST)	Lon.	Lat.	Depth [km]	M_{rr}	$M_{\theta\theta}$	$M_{\phi\phi}$	$M_{r\theta}$	$M_{r\phi}$	$M_{\theta\phi}$	Exp.	Mw	VR [%]
2004-09-05T19:07:13	136.7	33	26	3.4335	-4.5007	1.0672	-0.1465	0.4235	0.4357	26	7.01	70.9
2004-09-05T23:57:42	137	33.2	20	0.8675	-1.1077	0.2402	-0.3706	0.1465	0.1220	27	7.29	71.8